A: Kinetics, Dynamics, Photochemistry, and Excited States

Photo-Oxidation Reactions of Ethyl 2-Methyl Propionate (E2MP) and Ethyl-2,2- Dimethyl Propionate (E22DMP) Initiated by OH Radicals: An Experimental and Computational Study

Revathy Kaipara, and Balla Rajakumar

Just Accepted

Photo-Oxidation Reactions of Ethyl 2-methyl propionate (E2MP) and Ethyl-2,2-dimethyl propionate (E22DMP) Initiated by OH radicals: An Experimental and Computational study

Revathy Kaipara and B. Rajakumar*

Department of Chemistry, Indian Institute of Technology Madras, Chennai - 600036, India

*Address for correspondence: rajakumar@iitm.ac.in

http://chem.iitm.ac.in/faculty/rajakumar/

ABSTRACT

Relative Rate (RR) technique was used for the measurement of OH-initiated photo-oxidation reactions of Ethyl 2-methyl propionate (E2MP) and Ethyl-2,2-dimethyl propionate (E22DMP) in the temperature range of 268-363 K at 760 Torr. In addition to this, the thermodynamic and kinetic parameters for the title reactions were theoretically investigated using CCSD(T)/cc-pVTZ//M06-2X/6-311++G(2d,2p) level of theory in the temperature range of 200-400 K using Canonical Variational Transition State theory (CVT) in combination with Small Curvature Tunneling (SCT) method. The rate coefficients at (298±2) K were measured to be $k_{E2MP + OH} = (2.71±0.79) \times 10^{-12}$ cm^3 molecule^{-1} s^{-1} and $k_{E22DMP + OH} = (2.58±0.80) \times 10^{-12}$ cm^3 molecule^{-1} s^{-1}. The degradation mechanisms for the title reactions were investigated in the presence of O$_2$ using Gas Chromatography with Mass Spectrometry (GC-MS) and Gas Chromatography with Infrared Spectroscopy (GC-IR). From the recognized products, the possible product degradation mechanisms were predicted. In addition to this, the atmospheric lifetimes (ALs), lifetime-corrected Radiative Forcing (RF), Global Warming Potential (GWPs) and Photochemical Ozone Creation

Potentials (POCPs) were calculated to further understand the environmental impact of these molecules on the Earth's troposphere.

1.Introduction

In the Earth's atmosphere, Oxygenated Volatile Organic Compounds (OVOCs) are emitted from both anthropogenic as well as biogenic sources.[1] OVOCs undergoes innumerable chemical and physical processes, leading to their conversion or exclusion from the atmosphere. Biogenic production of OVOCs along with global anthropogenic release of all nonmethane VOCs is about 200 Tg yr^{-1}.[2,3] Removal of OVOCs happens via photolysis and wet/dry deposition.[4,5] Majority of the OVOCs have low Henry's law constants (below 10^3 M atm^{-1}), signifying that, they will partition into the gas phase.[6] Ethyl 2-methyl propionate (E2MP) and ethyl-2,2-dimethyl propionate (E22DMP), categorized as OVOCs are fatty acid derivatives of methyl alkyl ester. They are present in alcoholic beverages and fruits such as apple, banana, orange, wine grape, strawberry and nectarine.[7] A major concentration of these esters was also detected in the food flavoring agents.[8] In Earth's atmosphere, these esters are generated *in situ* via the oxidation of ethers.[9-11] Therefore, the emission of these OVOCs into the Earth's atmosphere from various sources, produces ground level pollutants, tropospheric ozone and secondary organic aerosols (SOAs).[12-16] The formation of SOAs and tropospheric ozone during the atmospheric oxidation of organic compounds are assessed globally at 20-380 Tg yr^{-1} and 4500 Tg yr^{-1} respectively.[18] This causes a significant rise in the concentration of emitted greenhouse gases, which in turn affect the global climate. Hence, the widespread use of these OVOCs in the various applications inevitably results in fugitive emission of these molecules into the Earth's atmosphere. The most of OVOCs are oxidized in the Earth's atmosphere via chemical reactions.[19] The deterioration of saturated OVOCs are initiated by their reaction with atmospheric oxidants. The degradation of OVOCs in the

troposphere leads to the production of secondary pollutants, such as ozone, VOCs, peroxyacyl nitrates, and SOA.[20] Therefore, the oxygen containing compounds play a significant role in defining the oxidizing capacity of the troposphere both on a local and a worldwide scale.

The emitted OVOCs are mainly removed via the photo-oxidation reactions with cleansing agents (like OH and NO_3 radicals, Cl atoms and O_3 molecules).[21] Although, their Cl-initiated kinetics is an order of magnitude higher than their reaction towards OH radicals. The low global concentration of Cl atoms (1×10^3 atoms cm^{-3})[22-28], when compared to that of OH radicals (1×10^6 molecules cm^{-3}) reduces the atmospheric significance of Cl atom-initiated reactions.[29] However, in coastal areas, Cl atom-initiated kinetics of OVOCs is significant. Moreover, in the troposphere, OH radical is considered to be the dominant oxidizing agent.[30,32] Therefore, OH-initiated photo-oxidation reactions mainly determine the atmospheric fate of these molecules. The production cycle for the tropospheric OH radical is because of the reaction of $O(^1D)$ formed from the UV-photolysis of O_3 with water vapor.[33-38] Till date, the kinetics of E2MP and E22DMP with OH radicals has not been investigated, so far. Therefore, this is the first investigation on the temperature-dependent kinetics of E2MP (R1) and E22DMP (R2) towards OH radicals in T = 268-363 K and at N_2 pressure of 760 Torr using RR technique coupled with Gas–Chromatography/Flame Ionization Detector (GC-FID). In addition to this, the kinetics was also calculated in T = 200-400 K using the geometries and energies obtained at CCSD(T)/cc-pVTZ//M06-2X/6-311++G(2d,2p) level of theory. The involved H-abstraction reaction pathways are depicted below, where a, b and c are the respective H-abstraction from the same reactive site.
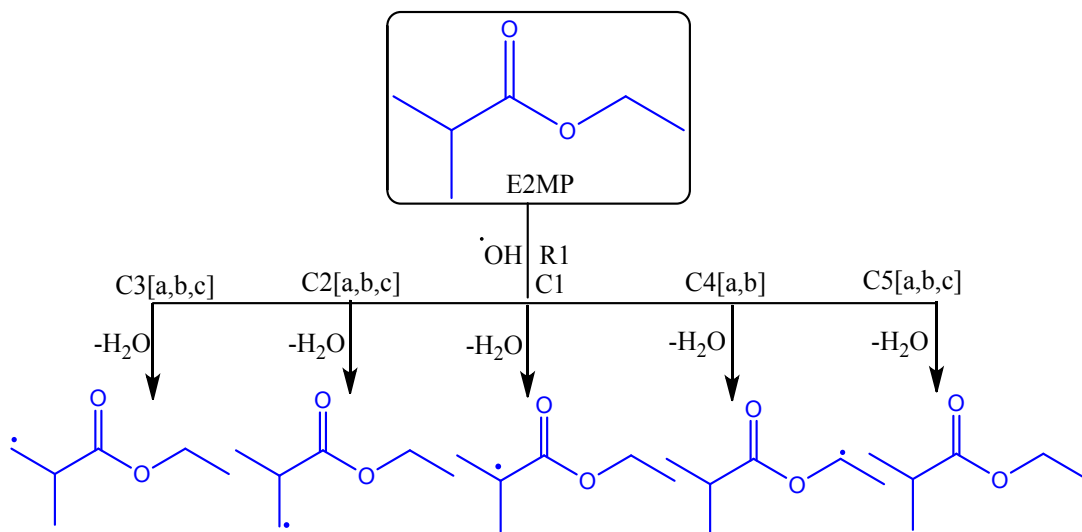
Scheme 1a. H-abstraction reaction channels include in the reaction of E2MP with OH radicals.
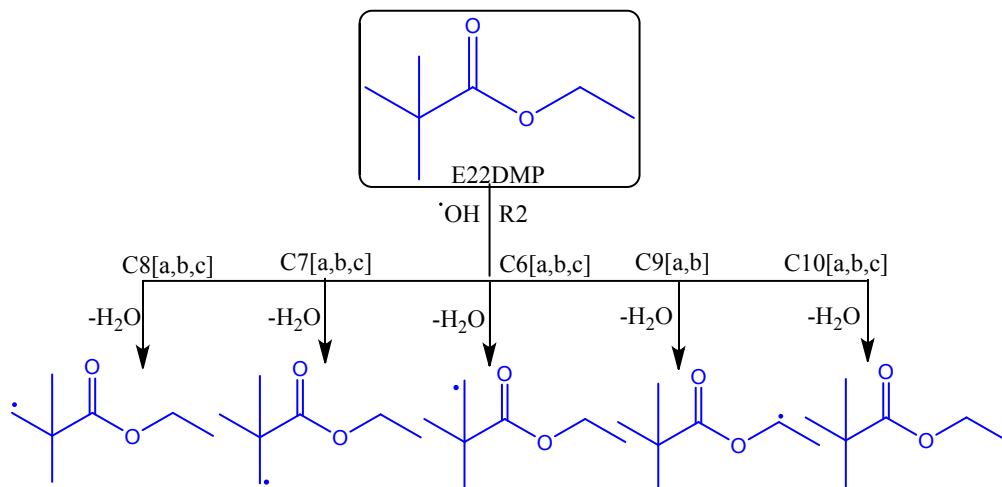
Scheme 1b. H-abstraction reaction channels include in the reaction of E22DMP with OH radicals.

The product analyses were studied using GC with Mass Spectrometer (GC-MS) and Infrared

Spectroscopy (GC-IR). To further comprehend their tropospheric impact, atmospheric lifetimes,

RFs, Global Warming Potential (GWPs) and Photochemical Ozone Creation Potentials (POCPs)
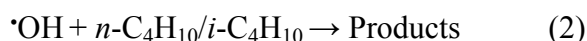
were calculated.

2. Methodology

2.1 Experimental details

Kinetics for R1 and R2 were measured in between 268-363 K and at 760 Torr of N_2. A doubled walled Pyrex glass cell of 100 cm length and 2.4 L volume was used to perform all the experiments over various temperatures, 268 K, 283 K, 298 K, 313 K, 343 K and 363 K. Temperature inside the reaction cell was maintained using Julabo (a thermostat), which circulates heated or cooled fluid inside the double jacked wall. Calibration of the cell temperature was performed using a K-type thermocouple and a ±2 K in the uncertainty was found. Photolysis of H_2O_2 (a precursor for OH radicals) was done using a KrF Excimer laser with λ_{max} = 248 nm (Coherent COMPEX Pro 102F). The concentration of H_2O_2 in the reaction cell was varied in the range of (4-6) × 10^{17} molecule cm^{-3}. The detailed experimental set up and the related procedure are available in our previous publications.[39,40] Reference compounds used were butane (n-C_4H_{10}) or iso-butane (i-C_4H_{10}) respectively.

Reaction chamber consists of a mixture of sample molecule (E2MP or E22DMP), H_2O_2 and a reference compound. The initial concentrations of the sample and reference compounds were varied in the range of (3-6) × 10^{16} molecule cm^{-3}. Concentration of the reaction mixture was monitored using GC-FID (Agilent technologies, 7890 B). Separation of the gaseous species was acquired using HP-PLOTQ capillary column (30 m × 0.32 mm × 20 μm). The GC-oven temperature and the flow rate were maintained at 220 $^{\circ}$C and 3 mL min^{-1}. To further verify the influence of secondary reactions or dark reactions, the reaction mixture ((E2MP/E22DMP) + reference + H_2O_2) was kept for 2-3 hours with no photolysis source. After a certain time, the concentrations were analyzed and was found to depict no change in the concentrations. Hence, dark reactions do not contribute to a significant extent. In addition to this, to check the interference

of secondary reaction in the absence of H_2O_2, the reaction mixture (E2MP/E22DMP) + reference) was photolyzed and kept for 2-3 hours. After that, the analysis of the concentration led to the conclusion that, the concentrations of the sample molecules or the reference compounds did not show significant variation. The Figures of these control experiments are shown in Figure S1 of the Supporting Information (SI). Thus, the intrusion of any secondary chemistry inside the reaction cell was insignificant and it was also confirmed that, the decay in the concentration of the sample and reference is merely due to their reactivity towards OH radicals.

$$^\bullet OH + E2MP/E22DMP \rightarrow Products \qquad (1)$$

$$^\bullet OH + n\text{-}C_4H_{10}/i\text{-}C_4H_{10} \rightarrow Products \qquad (2)$$

Measurement of the temperature-dependent kinetics was procured from the instantaneous loss of the sample and the reference using the following expression:

$$\ln\left(\frac{\{Ester\}_0}{\{Ester\}_t}\right) = \frac{k_{Ester}}{k_{ref}} \ln\left(\frac{\{ref\}_0}{\{ref\}_t}\right) \qquad (3)$$

where, [Ester]$_0$, [ref]$_0$, [Ester]$_t$, and [ref]$_t$ are the concentrations of E2MP, E22DMP and reference compounds at times t_0 and t, and k_{Ester} and k_{ref} are the rate coefficients of the sample molecules and reference compounds. Plot of $\ln\left((Ester)_0/(Ester)_t\right)$ vs $\ln\left((ref)_0/(ref)_t\right)$ is expected to yield a straight line with zero intercept, indicating the absence of secondary chemistry on the measured kinetics over the studied temperature range. The ratio $\left(\frac{k_{Ester}}{k_{ref}}\right)$ obtained can be multiplied by k_{ref}, which would yield the k_{sample} at a particular temperature.

2.2. Product analysis

The product analyses were studied using GC-MS (GCMS-5977A-MSD, Agilent technologies) and GC-IR (GC (7890B, Agilent technologies)-IR (Thermo scientific IS50)-MCT). HP-PLOTQ

column was used for the separation of the eluted products. The oven temperature of the two instruments was varied from 30 °C to 250 °C with a temperature rate of 5 °C min^{-1}. The source and the MS Quad temperature were kept at 150 °C and 200 °C respectively. All the GC-IR experiments were obtained with a spectral resolution of 4 cm^{-1}.

Purity of the chemicals as listed by the manufactures is given here, E2MP and E22DMP (99%, Aldrich), H_2O_2 (98%, Spectrochem), n-C_4H_{10}, i-C_4H_{10}, N_2 and O_2 (98%, Bhuruka gases) and He (99.999%, Praxair). The esters were purified before their use through several cycles of freeze-pump-thaw.

2.3. Computational Methodology

A meta-hybrid functional, M06-2x (with 54 % HF exchange)[41-43] coupled with Pople's basis set 6-311++G(2d,2p) (MG3S)[44,45] was used for the optimization of the reactants (E2MP and E22DMP), transition states (TSs) and products (P$_i$). The use of M062x method in combination with MG3S basis set is known to have the best performance, and it is selected for use for direct dynamics calculations[46-51]. Individually, both the M06-2x method as well as the MG3S basis set[52] are known to be good for the computation of accurate barrier heights and thermodynamic parameters. Details of the computational methodology are specified in Section 1 of the SI.

3. Results and discussion

3.1. Kinetics Measurements

Rate coefficients (k in cm^3 molecule^{-1} s^{-1}) were measured with respect to n-butane (n-C_4H_{10}) and iso-butane (i-C_4H_{10}). The reported rate coefficients of the reference compounds at 298 K are, $k_{n\text{-}C4H10+OH}$ = (2.36±0.47) × 10^{-12} and $k_{i\text{-}C4H10 + OH}$ = (2.12±0.42) × 10^{-12}.[53] Relative rate plots for R1 and R2 are given in Figures 1a and 1b. The slopes obtained from the relative plots and the average

rate coefficient (k_{avg}) calculated at each temperature are listed in Tables 1a and 1b. The errors

quoted are the 2σ statistical errors obtained by fitting the kinetic data using the linear least squares

method and the reported uncertainties in the reference rate coefficients. The details about the error

analysis are given in Section -2 of the SI.

The kinetics (in units of cm^3 molecule^{-1} s^{-1}) was fitted to the linear least squares method and the

Arrhenius expression were obtained as, $k_{R1}^{268-363\ K} = [(4.15\pm0.87) \times 10^{-13} \exp (568.3\pm64.5)/T]$ and

$k_{R2}^{268-363\ K} = [(4.24\pm0.92) \times 10^{-13} \exp (548\pm66)/T]$. A negative dependence of the kinetics on the

temperature was observed and the respective Arrhenius plots are shown in Figures 2a and 2b. The

298 K rate coefficients were obtained as, $k_{R1}^{298\ K} = (2.71\pm0.79) \times 10^{-12}$ and $k_{R2}^{298\ K} = (2.58\pm0.80)$

$\times 10^{-12}$ respectively.

3.2. Computational section

3.2.1. Reaction energetics

Optimized stationary points obtained at the studied level of theory for both the reactions R1 and

R2 as well as the respective Potential Energy Surfaces (PESs) are shown in Figure 3, Figures 4a

and 4b. The calculated thermochemical parameters (such as $\Delta G°$ and $\Delta H°$ in the units of kcal mol^{-1})

for both the reactions R1 and R2 are listed in Tables 2a and 2b. It can be understood from the

Tables 2a and 2b that, all the H-abstraction reaction channels in E2MP (C1[a,b,c] – C5[a,b,c]) and

E22DMP (C6[a,b,c] – C10[a,b,c]) were found to be exothermic ($\Delta H°< 0$) and spontaneous ($\Delta G°$

< 0). The reaction channel C1 ($\Delta H°$=-28.5 and $\Delta G° = -29.8$) in E2MP and C9[a, b] ($\Delta H°= -20.1$

and $\Delta G° = -21.2$) in E22DMP were found to be thermodynamically more facile, when compared

to other H-abstraction reaction routes. Schematic representations of all the TSs involved in the

reactions R1 and R2 are shown in Scheme 1c and 1d.

Scheme 1c
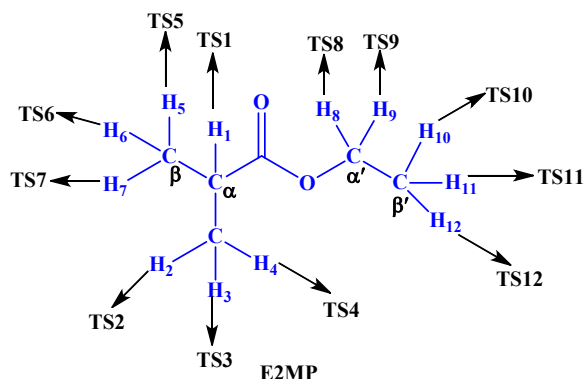
Scheme 1c. Plausible H-abstraction TSs in the reaction of E2MP with OH radicals.

It is clear from the PES in Figure 4a that, the abstraction of H_1 atom by OH radical from the α-carbon in C1 via TS1 was found with a $\Delta E^{\ddagger}$ value of 3.0 kcal mol^{-1}. The three methyl hydrogens (H_2, H_3 and H_4) attached to the α-carbon were non-equivalent, due to their spatial arrangement. Therefore, TS2, TS3 and TS4 were found with $\Delta E^{\ddagger}$ values (in units of kcal mol^{-1}) of 6.2, 3.3 and 4.9. Similarly, the three H-atoms (H_5, H_6 and H_7) at the β-carbon were non-equivalent. Hence, TS5, TS6 and TS7 were observed with $\Delta E^{\ddagger}$ values (in units of kcal mol^{-1}) of 4.3, 3.3 and 6.5. The two H-atoms (H_8 and H_9) at the α'-carbon via TS8 and TS9 with $\Delta E^{\ddagger}$ values of 2.5 kcal mol^{-1} were found to be equivalent. The three H-atoms (H_{10}, H_{11} and H_{12}) at the β'-carbon were non-equivalent, due to their 3D-orientation. Therefore, TS10, TS11 and TS12 were identified with $\Delta E^{\ddagger}$ values (in units of kcal mol^{-1}) of 7.7, 6.0 and 4.6. All the TSs (TS1-TS12) were located via the elongation of the breaking C-H bond by 12-14% and a compression of O-H bond distances by 39-43%. To further comprehend the nature of the TSs, L-parameter[54] values were calculated and are shown in Table 2a, suggested that, all the TSs depict reactant-like nature or are early TSs.

Scheme 1d
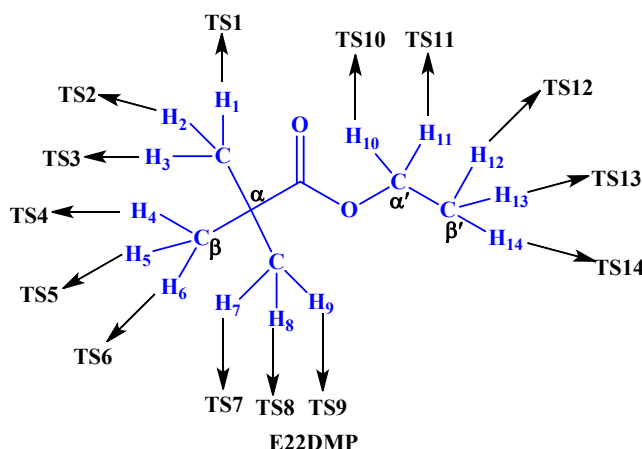
Scheme 1d. Plausible H-abstraction TSs in the reaction of E22DMP with OH radicals.

From the PES displayed in Figure 4b and the Scheme 1b revealed that, one of the H-atoms (H_1) at the $-CH_3$ group attached to the α-carbon was different from H_2 and H_3, due to their stereographical orientation. Hence, TS1 was located with a $\Delta E^{\ddagger}$ value of 0.6 kcal mol^{-1}, while TS2 and TS3 were equivalent with $\Delta E^{\ddagger}$ values of 5.4 kcal mol^{-1}. Similarly, H_6 attached to the $-CH_3$ group at the β-carbon was dissimilar to H_4 and H_5. Hence, TS4 and TS5 were equivalent with $\Delta E^{\ddagger}$ value of 0.8 kcal mol^{-1}, whereas TS6 was located with a $\Delta E^{\ddagger}$ value of 2.8 kcal mol^{-1}. Furthermore, H_7, H_8 and H_9 at the $-CH_3$ group attached to the α-carbon were non-equivalent, due to their stereographical orientation. Therefore, TS7, TS8 and TS9 were located with $\Delta E^{\ddagger}$ values (in units of kcal mol^{-1}) of 0.5, 0.8 and 2.2. H_{10} and H_{11} at the α'-carbon were equivalent and with $\Delta E^{\ddagger}$ value of -0.2 kcal mol^{-1}. H_{13} attached to the β'-carbon was dissimilar to H_{12} and H_{14}. Therefore, TS12 and TS14 were equivalent with $\Delta E^{\ddagger}$ value of 3.3 kcal mol^{-1}, whereas TS13 was observed with a $\Delta E^{\ddagger}$ value of 4.7 kcal mol^{-1}. All the TSs (TS1-TS14) were located along the MEP with a C-C bond elongation of 10-12% and an equivalent O-H bond length compression by 39-44%. Moreover, it was evident

from Table 2b that, L-parameter[54] values for all the TSs were found to be less than one. Thus, all the TSs are early TSs or exhibit reactant-like nature.

3.2.2. Rate coefficient calculations

The kinetics for the reactions R1 and R2 were calculated using CVT/SCT method and are listed in Table 3. In reaction R1, C4[a,b] via TS8 and TS9 was found to be kinetically labile reaction channel.

The global rate coefficient for the reaction R1 was obtained by adding the distinct rate coefficients obtained for individual H-abstraction reaction channels (listed in Table S5) as shown below,

$$k_{R1}^{total} = k_{C1} + k_{C2[a,b,c]} + k_{C3[a,b,c]} + k_{C4[a,b]} + k_{C5[a,b,c]} \tag{4}$$

The Arrhenius expression was acquired by performing a non-linear fit to the calculated rate coefficients (k in cm^3 molecule^{-1} s^{-1}) and the respective Arrhenius plot is shown in Figure 2a. The overall rate coefficient for R1 at 298 K was calculated to be $k_{R1}^{298\,K}$= 3.01×10^{-12} and the temperature-dependent expression was obtained as, $k_{R1}^{200-400\,K}$= 6.15×10^{-21} T$^{2.70}$ exp[(1384/T)] cm^3 molecule^{-1} s^{-1}. The rate of the reaction decreases in magnitude, as the temperature increases. It is evident from the Figure 2a that, the computed rate coefficient at 298 K was found to be in good agreement with the measured value ($k_{R2.3}^{298\,K,\ measured}$= (2.71±0.79)×10^{-12} under the experimental error limits.

In the case of the reaction R2, reaction channel C9[a,b] via TS10 and TS11 was both thermodynamically favored and kinetically feasible. The total rate coefficient was calculated by the addition of the individual rate coefficients (given in Table S6) involved in reaction R2 using the following formula,

$$k_{R2}^{total} = k_{C6[a,b,c]} + k_{C7[a,b,c]} + k_{C8[a,b,c]} + k_{C9[a,b]} + k_{C10[a,b,c]} \tag{5}$$

A nonlinear fit to the computed rate coefficients was performed to obtain the Arrhenius plot given in Figure 2b. The total rate coefficient for R2 at 298 K was obtained as, $k_{R2}^{298\ K}= 2.82\times10^{-12}$ and the Arrhenius expression was obtained as, $k_{R2}^{200\ -\ 400\ K}= 3.88\times10^{-27}$ T$^{4.93}$ exp[(1806/T)] cm^3 molecule^{-1} s^{-1}. Overall, the rate decreased, as the temperature rises from 200 to 400 K. It is evident from Figure 2b that, the computed room temperature rate coefficient was in good agreement with the measured rate coefficient ($k_{R2}^{298\ K,\ measured}= (2.58\pm0.80) \times 10^{-12}$), under the experimental error limits.

3.3. Branching ratios (BRs)

BRs for the title reactions were estimated to understand the impact of individual reaction channel (k_i) to the total rate of the reactions (k_{total}) and are calculated using the following expression,

$$\text{Branching ratios (\%)} = \frac{k_i}{k_{total}}\times100 \qquad (6)$$

The role of each reaction route to the global kinetics of the reactions R1 and R2 are shown in Figures 5a and 5b. It is obvious from the Figure 5a that, the contribution of C4[a,b] via TS8 and TS9 was found to decrease, as temperature increases from 200 K (45 %) to 400 K (31 %). On contrary, the contributions of other TSs increased with an equivalent rise in the temperature. Therefore, these TSs were minor contributors to the total reactivity of E2MP towards OH radicals, when compared to the major reaction channel. Hence, reaction channel C4[a,b] was the dominant contributor to the total reaction.

Moreover, it can be understood from the Figure 5b, the BR of the TS10 and TS11 via reaction channel C9[a, b] was the major contributor to the total reactivity. Further, it can be seen that, the contribution of TS10 and TS11 decreased from 67% to 20% with an increase in temperature from

200 to 400 K. On the other hand, the contribution of TS13 increased with an increase in the temperature. After 313 K, TS13 was the major contributor to the global reactivity. Furthermore, the BRs of other TSs increased with an increase in the temperature. However, these TSs were minor contributors to the total reactivity, when compared to the dominant TSs. Therefore, reaction channel C9[a,b] is the major contributor in the reactivity of E22DMP towards OH radicals.

3.4. Reactivity trends

Based on the available literature, it was corroborated that, no prior kinetic study was carried out for reactions R1 and R2. Hence, the current work is the first attempt to investigate these reactions and thus, direct comparison to the available literature cannot be attained. However, the kinetics measured in this work were compared with the rate coefficient of the analogues molecules (MP, M2MP and EP). The rate coefficients measured in this work and the reported rate coefficients of the analogues molecules at 298 K are given in Table 4. As seen from the Table 4 that, the reactivity of M2MP towards OH radical was found to be higher than that of the reactivity of MP towards OH radicals. This difference in the reactivity can be better explained in terms of the radical stability, deactivating group and hyperconjugation effects. Mendes et al.[55] theoretically investigated the kinetics for the reactions of MP and M2MP with OH radical and explained that, the H-abstraction from the α-position attached to the ester moiety (RC(O)OR') happens in a similar way, due to the electron delocalization of RC(O)OR' group. So, the effect of deactivating group was found to be insignificant. Furthermore, the radical stability increases in the order of -$CH_3 < 1° < 2° < 3°$ group. Moreover, higher the number of alkyl substituents on the radical bearing carbon, more is the stabilization energy, due to the hyperconjugation effect. Hence, the H-abstraction by OH radical from M2MP formed the 2° radical, whereas, in the case of MP, the formation of 1° radical was noted to be the major reaction channel. This in turn explained the

increase in the reactivity of the M2MP, when compared to the reaction of MP towards OH radicals.

Similarly, the reactivity of EP[56] and E2MP towards OH radical can also be explicated. However, it is important to know that, the dominant reaction sites for the reaction of E22DMP with Cl atoms and OH radicals were the abstraction of the hydrogen atoms attached to the acetoxy side ($-OCH_3-$). Therefore, the reactivity of E22DMP is comparable, even though the OH-based kinetics was an order of magnitude different, when compared to the respective Cl-initiated kinetics. Ifang et al.[57] investigated the kinetics for the reaction of E22DMP with Cl atom and observed a small discrepancy in the overall kinetics, due to the reactivity of $-CH_x-$ ($x = 1,2,3$) moiety, which influences both the α and β positions attached to the acyl group ($-C(O)OR$). It is also well-known that, for the reaction of OH radical with oxygen-rich compounds, ester moiety can alter the reactivity of the $-CH_x-$ groups on both the sides, up to δ position.[13]

In addition to this, the reactivity of the studied esters towards OH radical were compared based on the SAR method given by Kwok and Atkinson.[58] The authors assumed that, the rate constants for the H-abstraction from the C-H bond of the molecules is based on the estimation of the group rate constants from the $-CH_3$, $-CH_2$ and $-CH<$ moieties and are defined as,

$$k(CH_3-X) = k_{prim}\ F(X),$$

$$k(X-CH_2-Y) = k_{sec}\ F(X)\ F(Y),\ \text{and}$$

$$k(X-CH-Y(Z)) = k_{tert}\ F(X)\ F(Y)\ F(Z),$$

where, k_{prim}, k_{sec} and k_{tert} are the rate coefficient of $-CH_3$, $-CH_2$ and $-CH<$; X, Y and Z and F(X), F(Y) and F(Z) are the substituent group and factors, where $F(-CH_3) = 1.00$, $F(-CH_2) = F(-CH<) = 1.23$, $F(C(O)OR) = 0.74$, and $F(-C(O)O-) = 1.6$. Based on this, k (in cm^3 molecule^{-1} s^{-1}) for the reactions R1 and R2 were calculated as, $k_{R1}^{298\ K,\ SAR} = 3.80 \times 10^{-12}$ cm^3, and $k_{R2}^{298\ K,SAR} = 1.72 \times 10^{-12}$

respectively. From this kinetic data, it was concluded that, the measured ones ($k_{R1}^{298\ K,measured}=$

$(2.71\pm0.79)\times10^{-12}$ and $k_{R2}^{298\ K,measured}=$ $(2.58\pm0.80)\times10^{-12}$), and the calculated kinetic data (

$k_{R1}^{298\ K,\ calculated}=$ 3.01×10^{-12} and $k_{R2}^{298\ K,\ calculated}=$ 2.82×10^{-12}) were in reasonable agreement

with the SAR-based rate coefficients.

3.5. Product analysis

The product analyses for the reactions R1 and R2 were studied using GC-MS and GC-IR. The

obtained chromatograms are shown in Figures 6a and 6b. Based on the product analyses, possible

product degradation mechanisms were predicted and are shown in Figures 7a and 7b. The

individual MS and IR-absorption spectra of all the products are given in Figures S4 and S5.

In the case of reaction R1, reaction channel (C4[a,b]) was found to be kinetically dominant

pathway. Hence, CH_3CHO formed from this channel was found to be the major degradation

product. This product was formed due to the interaction of OH radical towards the α'-carbon in the

presence of O_2, followed by recombination reaction to form the $(CH_3)_2CHC(O)OCH^{\bullet}CH_3$ radical.

Further, this alkoxy radical undergoes $C_{\alpha'}$-O decomposition to form CH_3CHO and

$(CH_3)_2CHC(O)O^{\bullet}$ radical. Later, this radical undergoes C_{α} -C(O) bond scission to form CO_2 and

1-propene ($CH_3CH=CH_2$) as products. Cavalli et al.[59] explained the formation of peroxy radical in

their product study for the reaction of methyl propionate with OH radical due to the reaction of

alkyl radical with O_2. Author also illustrated the formation of alkoxy radical due to the self-reaction

of peroxy radical followed by its decomposition to yield various products. There are several other

literatures also explained the formation of alkoxy radical and its further degradation to form

various products.[60-62] The formation of these products was confirmed with *m/z* ratios at 32, 37, and

44 for CH_3CHO; and 29, 39, 40, 42 and 43 for $CH_3CH=CH_2$. The IR- peak at 2850 cm^{-1} (C-H

stretch) and 1725 cm^{-1} (C=O stretch) for CH$_3$CHO; and 3083 cm^{-1} (=C-H stretch), 2966-2960 cm^{-1} (C-H stretch in alkane), 1654 cm^{-1} (C=C bond) and 675-990 cm^{-1} (bending =C-H stretch) and 1465 cm^{-1} (C-H scissoring) for CH$_3$CH=CH$_2$ also confirmed the formation of these products. Furthermore, CH$_3$CHO and ethyl formate (HC(O)OCH$_2$CH$_3$) were also observed as one of the degraded products, due to the elimination of methyl group in the presence of O$_2$, followed by the recombination reaction and C-C bond fission of the corresponding radical. HC(O)OCH$_2$CH$_3$ was confirmed with *m/z* ratios at 31, 38, 43, 48, 56 and 74; and IR-peaks at 2967 cm^{-1} (C-H stretch), 1726 cm^{-1} (C=O stretch), 1206 cm^{-1} (C-O stretch) and 842 cm^{-1} (O-C(O)). In addition to this, other minor products were observed, due to the approach of OH radical towards α-carbon in reaction channel (C1). (CH$_3$)$_2$C$^•$C(O)OCH$_2$CH$_3$ radical was formed from the H-abstraction by OH radical via C1. After that, this radical reacts with O$_2$ and formed (CH$_3$)$_2$COO$^•$C(O)OCH$_2$CH$_3$ radical. This unstable alkyl peroxy radical undergoes self-reaction to produce alkoxy (CH$_3$)$_2$CO$^•$C(O)OCH$_2$CH$_3$ radical. Later, this alkoxy radical undergoes C$_\alpha$-C(O) decomposition to form CH$_3$C(O)CH$_3$ and $^•$C(O)OCH$_2$CH$_3$ radial. Further, this radial undergoes O-C$_{\alpha'}$ cleavage in the presence of O$_2$ to form HCHO and CH$_3$OH as products. Ifang et al.[57] studied the product analysis of methyl-2-methyl propionate with Cl atom in the presence of O$_2$ and explained the formation of acetone by the decomposition of corresponding alkoxy radical. The formation of these products was recognized with *m/z* ratios at 29, 28 and 30 for HCHO; 43, 58, 38 and 30 for CH$_3$C(O)CH$_3$; and 15, 30, 31 and 32 for CH$_3$OH. The IR- peaks at 2964 cm^{-1} (C-H stretch), 1659 cm^{-1} (C=O stretch) and 842 cm^{-1} (O-C(O) stretch) for HCHO; and 1716 cm^{-1} (C=O stretch) for CH$_3$C(O)CH$_3$; and 3200-3600 cm^{-1} (strong and broad O-H stretch), 3510-3678 cm^{-1} (strong and sharp O-H stretch) and 1055-1148 cm^{-1} (C-O stretch) for CH$_3$OH also confirmed the formation of these products.

In the case of reaction R2, acetaldehyde was formed due to the interaction of OH radical towards the α'-carbon (C9[a,b]) in the presence of O_2, followed by the self-reaction to form corresponding alkoxy radical $((CH_3)_2CHC(O)OCHO^•CH_3)$. Further, this radical undergoes decomposition reaction to form CH_3CHO and $(CH_3)_2CHC(O)O^•$ radical. Later, this radical undergoes -C-C(O) cleavage to form 2-methyl 1-propene $((CH_3)_2CH=CH_2)$ and CO_2. The products were identified with *m/z* ratios at 32, 37 and 44 for CH_3CHO; and 37, 38, 39, 41, 42, 55 and 56 for $(CH_3)_2CH=CH_2$. The IR-peaks at 2850 cm^{-1} and 2750 cm^{-1} (C-H stretch) and 1725 cm^{-1} (C=O stretch) for CH_3CHO; and 3010-3100 cm^{-1} (medium =C-H stretch), 1620-1680 cm^{-1} (variable C=C bond) and 675-990 cm^{-1} (bending =C-H stretch) for $(CH_3)_2CH=CH_2$ also confirmed the formation of these products. Moreover, some minor products were also observed from the product analysis, due to the approach of OH radical towards the methyl group attached to the α-carbon. HCHO and $(CH_3)_2O^•CHC(O)OCH_2CH_3$ radical were formed, due to the H-abstraction by OH radical from the methyl group attached to the α-carbon in the presence of O_2. HCHO was confirmed with *m/z* ratios at 29, 28 and 30; and IR- peaks at 2964 cm^{-1} (C-H stretch),1659 cm^{-1}-1518 cm^{-1} (C=O stretch) and 842 cm^{-1} (O-C(O) stretch). Further, the -C-C(O) bond scission from the $(CH_3)_2O^•CHC(O)OCH_2CH_3$ radical leads to the formation of acetone $(CH_3C(O)CH_3)$ and $^•C(O)OCH_2CH_3$ radical. Wallington et al.[63] in their product study on the reaction of Cl atom with methyl-2,2dimethyl propionate and reported that the alkyl radical formed in their system was further oxidized to acetone. The formation of $CH_3C(O)CH_3$ was recognized with *m/z* ratios at 43, 58, 38 and 30; and IR-peaks at 1716 cm^{-1} (C=O stretch). After that, $^•C(O)OCH_2CH_3$ radical undergoes two different decomposition channels to give different products. First, the decomposition of $^•C(O)OCH_2CH_3$ radical leads to the formation of CO_2 and $CH_3CH_2^•$ radical. Later, methanol (CH_3OH) and HCHO were formed from the further decomposition of $CH_3CH_2^•$

radical in the presence of O_2. CH_3OH was identified with *m/z* ratios at 15, 30, 31 and 32; and IR-peaks at 3200-3600 cm^{-1} (strong and broad O-H stretch), 3510-3678 cm^{-1} (strong and sharp O-H stretch) and 1055-1148 cm^{-1} (C-O stretch). The other pathway involves the formation of ethyl formate ($HC(O)OCH_2CH_3$) and further reaction with OH radical followed by the HO_2 radical elimination to form acetic formic anhydride ($HC(O)OC(O)CH_3$). This product was recognized with *m/z* ratios at 31, 38, 43, 48, 56 and 74; and was not identified in GC-IR, because the concentration may be below the detection limit of the MCT detector of IR spectrometer.

3.6. Atmospheric implication

The kinetics measured in this work were used to determine the atmospheric lifetime of the studied esters. The atmospheric lifetimes (τ) with regard to OH radical were estimated using the expression, $\tau = 1/k[X]$, where 'k' is the rate coefficient for the reaction of E2MP and E22DMP with OH radical at 298K and 'X' is the global concentration of OH radical (1×10^6 molecule cm^{-3}).[64] By using this equation, the atmospheric lifetimes were estimated to be 92 hours for E2MP and 105 hours for E22DMP. In addition to this, to further understand their impact on the atmosphere, RFs, GWPs and POCPs were calculated and are shown in Table 5. RF was calculated using the method recommended by Pinnock et al.[65] They have assumed that the molecules are well-mixed in the Earth's atmosphere. However, the residence time of these studied molecules are not long enough for the vertical mixing. Hence, Hodneberg et al.[66] suggested a correction factor to determine the lifetime-corrected RF using the expression,

$$f(\tau) = \frac{a\tau^b}{1 + c\tau^d} \qquad (7)$$

where, *a*, *b*, *c* and *d* are constants with values of 2.692, 0.9312, 2.994 and 0.9302. Based on this explanation, the lifetime-corrected RF of E2MP and E22DMP were assessed to be 0.04 and 0.20.

The positive RF revealed that, these studied molecules do not contribute towards any significant warming in the Earth's atmosphere.[67] Moreover, by using the estimated value for the lifetime-corrected RF, GWPs for the studied esters were calculated using the following equation,

$$GWP = \frac{a\int_0^{TH} exp\left[-\frac{1}{\tau}\right]dt}{AGWP_{CO_2}} \qquad (8)$$

$$a = \sum_k A_k F(v_k) \qquad (9)$$

where, TH is the time horizon, a is the total infrared radiative forcing, $AGWP_{CO_2}$ is the global warming potential for CO_2. Further, to determine the GWPs, vibrational frequencies (v_k)[68] and intensities (A_k) of the studied molecules were obtained at the B3LYP/6-31+G(d, p) level of theory and were calculated in the time horizon of 20,100 and 500 years.[69, 70] As can be seen from the Table 5 that, the GWPs of the E2MP was found to be negligible, as compared to the GWPs of E22DMP. In the case of E22DMP, the GWPs in the time horizon of 20 years was calculated to be 3.9. According to the Intergovernmental Panel on Climate Change (IPCC) suggested that, the GWPs of the molecules were typically calculated with respect to CO_2 (GWPs =1).[15] Hence, the emission of E2MP into the Earth's atmosphere does not cause any significant change in the global warming, when compared to E22DMP.

3.7. Photochemical Ozone Creation Potentials (POCPs)

The POCPs for the studied esters were determined based on the method suggested by Jenkin et al.[71] and Derwent et al[72] and are listed in Table 5. The authors explained that, the POCP of a particular VOCs is determined by enumerating the consequence of a small incremental increase in its emanation on the calculated amount of ozone formed, comparative to an identical increase in

the O_3 release, due to a reference VOC (ethene). The expression used for the calculations is as follows,

$$POCP = \alpha_1 \times \gamma_s \times \gamma_R^{\beta}(1 - \alpha_2 \times n_c) \qquad (10)$$

where, α_1, β and α_2 are constants, γ_s is the structure-based ozone formation index, γ_R is the reactivity-based ozone formation index, and n_c is the number of carbon atoms. Further, the γ_s and γ_R for the molecules were calculated using the following equation,

$$\gamma_s = \left(\frac{n_B}{M}\right) \times \left(\frac{28}{6}\right) \qquad (11)$$

$$\gamma_R = \left(\frac{k_{OH}}{n_B}\right) \times \left(\frac{6}{k_{OH}^{ethene}}\right) \qquad (12)$$

Where, n_B is the number of C-C and C-H bonds, M is the molecular weight, k_{OH} is the rate coefficient for the reaction of molecules with OH radical at 298 K, k_{OH}^{ethene} is the rate coefficient for the reaction of ethene with OH radical at 298 K and was reported to be 8.64×10^{-12}.[71] Based on these values, the POCP of E2MP and E22DMP were calculated to be 33.9 and 30.9. These values suggested that, there will be a minimal formation of ozone in the Earth's troposphere from these studied molecules, when compared to ethene (100).

4. Conclusions

OH radical-initiated photo-oxidation reactions of E2MP and E22DMP were investigated, both experimentally and computationally. The computed thermodynamic parameters illustrated that, the H-abstraction by OH radical from the α'-position towards the acetoxy side (-C(O)OCH-) was found to be kinetically labile reaction channel for both the studied esters. The kinetic data revealed that, the reactivity of E2MP and E22DMP towards OH radical was found to be comparable with

each other. In the OH-initiated oxidation of studied esters in the presence of O_2, carbonyl compounds (such as HCHO, $CH_3C(O)CH_3$ and CH_3CHO) were formed as major oxidation products. Moreover, when compared to E22DMP, E2MP is short-lived and has low RF, which leads to low GWPs. Hence, the emission of E2MP into the Earth's troposphere is expected to have a minor impact on global warming and climate change.

Supporting Information

The cartesian coordinates and vibrational frequencies obtained for all the stationary points are listed in Tables S1 to S4, Control experiments to verify dark reactions are shown in Figure S1, IRC plots are shown in Figures S2 and S3, rate coefficients obtained for all the individual reaction pathways involved in the title reactions are given in Tables S5 and S6, the mass and IR spectra for all the products obtained from the degradation of title reactions are shown in Figures S4 and S5 and in Section-1 a complete explanation of computational methodology is described.

Acknowledgements

References

1) Calvert, J.; Mellouki, A. Mechanisms of atmospheric oxidation of the oxygenates. OUP USA. **2011**.

2) Mellouki, A.; Wallington, T.J.; Chen, J. Atmospheric chemistry of oxygenated volatile organic compounds: impacts on air quality and climate. *Chem. Rev.* **2015**, *115*, 3984-4014.

3) Wallington, T.J.; Seinfeld, J.H.; Barker, J.R. 100 years of progress in gas-phase atmospheric chemistry research. *Meteorological Monographs* **2019**, *59,* 10-1.

4) Dameris, M.; Loyola, D. Chemistry-climate connections–interaction of physical, dynamical, and chemical processes in Earth atmosphere. *Climate Change: Geophysical Foundations and Ecological Effects* **2011**, *3*.

5) Sander, R. Compilation of Henry's law constants for inorganic and organic species of potential importance in environmental chemistry (Version 3) **1999**.

6) Jagtap, U.B.; Bapat, V.A. Wines from fruits other than grapes: Current status and future prospectus. *Food Bioscience* **2015**, *9*, 80-96.

7) Helmig, D.; Müller, J.; Klein, W. Volatile organic substances in a forest atmosphere. *Chemosphere* **1989**, *19*, 1399.

8) Japar, S.M.; Wallington, T.J.; Richert, J.F.O.; Ball, J.C. The atmospheric chemistry of Oxygenated fuel additives: t-butyl alcohol, dimethyl ether, and methyl t-butyl ether. *Int. J. Chem. Kinet.* **1990**, *22*, 1257–1269.

9) Tuazon, E.C.; Carter, W.P.; Aschmann, S.M.; Atkinson, R. Products of the gas-phase reaction of methyl tert-butyl ether with the OH radical in the presence of NO_x. *Int. J. Chem. Kinet.* **1991**, *23*, 1003-1015.

10) Smith, D.F.; Kleindienst, T.E.; Hudgens, E.E.; McIver, C.D.; Bufalini, J.J. The photooxidation of methyl tertiary butyl ether. *Int. J. Chem. Kinet.* **1991**, *23*, 907–924.

11) El Boudali, A.; Le Calvé, S.; Le Bras, G.; Mellouki, A. Kinetic studies of OH reactions with a series of acetates. *J. Phys. Chem.* **1996**, *100,* 12364-12368.

12) Kanakidou, M.; Seinfeld, J.H.; Pandis, S.N.; Barnes, I.; Dentener, F.J.; Facchini, M.C.; Van Dingenen, R.; Ervens, B.; Nielsen, C.J. Organic aerosol and global climate modelling: a review. *Atmos. Chem. Phys.* **2005**, *5*, 1053–1123.

13) Mellouki, A.; Le Bras, G.; Sidebottom, H. Kinetics and mechanisms of the oxidation of oxygenated organic compounds in the gas phase. *Chem*. *Rev*. **2003**, *103*, 5077-5096.

14) Le Calvé, S.; Le Bras, G.; Mellouki, A. Kinetic studies of OH reactions with a series of methyl esters. *J. Phys. Chem. A* **1997**, *101*, 9137-9141.

15) Stocker, T.F.; Qin, D.; Plattner, G.K.; Tignor, M.; Allen, S.K.; Boschung, J.; Nauels, A.; Xia, Y.; Bex, V.; Midgley, P.M. Climate change: The physical science basis. Contribution of working group I to the fifth assessment report of the intergovernmental panel on climate change, **2013**, *1535*.

16) Haywood, J.; Boucher, O. Estimates of the direct and indirect radiative forcing due to tropospheric aerosols: A review. *Rev. Geophys.* **2000**, *38*, 513-543.

17) Fowler, D.; Amann, M.; Anderson, R.; Ashmore, M.; Cox, P.; Depledge, M.; Derwent, D.; Grennfelt, P.; Hewitt, N.; Hov, O.; Jenkin, M. Ground-level ozone in the 21st century: future trends, impacts and policy implications. **2008**, *15*, 08.

18) Wild, O. Modelling the global tropospheric ozone budget: exploring the variability in current models, **2007**.

19) Mellouki, A.; Le Bras, G.; Sidebottom, H. Kinetics and mechanisms of the oxidation of oxygenated organic compounds in the gas phase. *Chem. Rev.* **2003**, *103*, 5077-5096.

20) Mellouki, A.; Wallington, T.J.; Chen, J. Atmospheric chemistry of oxygenated volatile organic compounds: impacts on air quality and climate. *Chem. Rev.* **2015**, *115*, 3984-4014.

21) Finlayson-Pitts, B.J.; Pitts Jr, J.N., 1999. Chemistry of the upper and lower atmosphere: theory, experiments, and applications. *Elsevier* **1999**.

22) Vogt, R.; Crutzen PJ.; Sander R. A mechanism for halogen release from sea-salt aerosol in the remote marine boundary layer. *Nature* **1996**, *383*, 327–330.

23) Rudolph J.; Koppmann, R.; Plass-Dülmer, C. The budgets of ethane and tetrachloroethene: is there evidence for an impact of reactions with chlorine atoms in the troposphere? *Atmos. Environ.* **1996**, *30*, 1887–1894.

24) Singh, H.B.; Thakur, A.N.; Chen, Y.E.; Kanakidou, M. Tetrachloroethylene as an indicator of low Cl atom concentrations in the troposphere. *Geophys. Res. Lett.* **1996**, *23*, 1529–1532.

25) Spicer, C.W.; Chapman, E.G.; Finlayson-Pitts, B.J.; Plastridge, R.A.; Hubbe, J.M.; Fast, J.D.; Berkowitz, C.M. Unexpectedly high concentrations of molecular chlorine in coastal air. *Nature* **1998**, *394*, 353–356.

26) Thornton, J.A.; Kercher, J.P.; Riedel, T.P.; Wagner, N.L.; Cozic, J.; Holloway, J.S.; Dubé, W.P.; Wolfe, G.M.; Quinn, P.K.; Middlebrook, A.M.; Alexander, B.; Brown, S.S. A large atomic chlorine source inferred from midcontinental reactive nitrogen chemistry. *Nature* **2010**, *464*, 271–274.

27) Comes, F.J. Recycling in the Earth's atmosphere: The OH radical—its importance for the chemistry of the atmosphere and the determination of its concentration. *Angew. Chem.* **1994**, *33*, 1816-1826.

28) McKeen, S.A.; Trainer, M.; Hsie, E.Y.; Tallamraju, R.K.; Liu, S.C. On the indirect determination of atmospheric OH radical concentrations from reactive hydrocarbon measurements. *J. Geophys. Res. Atmos.* **1990**, *95*, 7493-7500.

29) Gligorovski, S.; Strekowski, R.; Barbati, S.; Vione, D. Environmental implications of hydroxyl radicals ($\cdot$OH). *Chem. Rev.* **2015**, *115*, 13051-13092.

30) Finlayson-Pitts, B.J.; Ezell, M.J.; Pitts, J.N. Formation of chemically active chlorine compounds by reactions of atmospheric NaCl particles with gaseous N_2O_5 and $ClONO_2$. *Nature* **1989**, *337*, 241-244.

31) Finley, B.D.; Saltzman, E.S. Measurement of Cl_2 in coastal urban air. *Geophys. Res. Lett.* **2006**, *33*, L11809.

32) Finley, B.D.; Saltzman, E.S. Observations of Cl_2, Br_2, and I_2 in coastal marine air. *Geophys. Res. Atmos.* **2008**, *113*, D21301.

33) Monks, P.S. Gas-phase radical chemistry in the troposphere. *Chem. Soc. Rev.* **2005**, *34*, 376.

34) Wennberg, P.O.; Salawitch, R.J.; Donaldson, D.J.; Hanisco, T.F.; Lanzendorf, E.J.; Perkins, K.K.; Lloyd, S.A.; Vaida, V.; Gao, R.S.; Hintsa, E.J.; Cohen, R.C. Twilight observations suggest unknown sources of HO_x. *Geophys. Res. Lett.* **1999**, *26*, 1373.

35) Salawitch, R.J.; Wennberg, P.O.; Toon, G.C.; Sen, B.; Blavier, J.F. Near IR photolysis of HO_2NO_2: Implications for HOx. *Geophys. Res. Lett.* **2002**. *29*, 9-1.

36) Dominé, F.; Shepson, P.B. Air-snow interactions and atmospheric chemistry. *Science* **2002**, *297*, 1506-1510.

37) Donaldson, D.J.; Frost, G.J.; Rosenlof, K.H.; Tuck, A.F.; Vaida, V. Atmospheric radical production by excitation of vibrational overtones via absorption of visible light. *Geophys. Res. Lett.* **1997**, *24*, 2651-2654.

38) Matthews, J.; Sinha, A.; Francisco, J.S. The importance of weak absorption features in promoting tropospheric radical production. *Proc. Natl. Acad. Sci. U.S.A.* **2005**, *102*, 7449.

39) Kumar, A.; Rajakumar, B. Cl atom-initiated photo-oxidation of mono-chlorinated propanes to form carbonyl compounds: A kinetic and mechanistic approach. *J. Phys. Chem. A* **2019**, *123*, 723-741.

40) Balan, R.C.; Balla, R. Cl-initiated photo-oxidation reactions of methyl propionate in atmospheric condition. *Environ. Sci. Pollut. Res.* **2018**, *25*, 20999-21010.

41) Zhao, Y.; Truhlar, D.G. The M06 suite of density functionals for main group thermochemistry, thermochemical kinetics, noncovalent interactions, excited states, and transition elements: two new functionals and systematic testing of four M06-class functionals and 12 other functionals. *Theor. Chem. Acc.* **2008**, *120*, 215-241.

42) Zhao, Y.; Truhlar, D.G. Density Functionals with broad applicability in Chemistry. *Acc. Chem. Res.* **2008**, *41*, 157−161.

43) Zhao, Y.; Truhlar, D.G. A new local density functional for main-group thermochemistry, transition metal bonding, thermochemical kinetics, and noncovalent interactions. *J. Chem. Phys.* **2006**, *125*, 194101.

44) McLean, A.D.; Chandler, G.S. Contracted Gaussian-basis sets for molecular calculations. 1. 2nd row atoms, Z=11-18. *J. Chem. Phys.* **1980**, *72*, 5639-5648.

45) Raghavachari, K.; Binkley, J.S.; Seeger, R.; Pople, J.A. Self-Consistent Molecular Orbitals Methods: Basis set for correlated wave-functions. *J. Chem. Phys.* **1980**, *72*, 650-654.

46) Wu, J.; Gao, L.W.; Ren, W.; Truhlar, D.G. Anharmonic kinetics of the cyclopentane reaction with hydroxyl radical. *Chem. Sci.* **2020**.

47) Zhang, R.M.; Truhlar, D.G.; Xu, X. Kinetics of the toluene reaction with OH radical. *Research* **2019**, 5373785.

48) Lynch, B.J.; Zhao, Y.; Truhlar, D.G. Effectiveness of diffuse basis functions for calculating relative energies by density functional theory. *J. Phys. Chem. A* **2003**, *107*, 1384-1388.

49) Saheb, V.; Bahadori, A. Theoretical studies on the kinetics of the hydrogen abstraction reactions from 1,3,5-trioxane and 1,4-dioxane by OH radicals. *Progress in Reaction Kinetics and Mechanism* **2020**, *45*, 1-13.

50) Xu, Q.; Kang, J.; Chen, X.; Li, J. Catalytic effect of water on the HO_3 + NO formations from the HNO + O_3 reaction in tropospheric conditions. *Molecular Simulations* **2020**.

51) Deka, R.C.; Mishra, B.K. Theoretical studies on kinetics, mechanism and thermochemistry of gas-phase reactions of HFE-449mecf with OH radicals and Cl atom. *J. Mol. Graph. Model.* **2014**, *53*, 23-30.

52) Zheng, J.; Xu, X.; Truhlar, D.G. Minimally augmented Karlsruhe basis sets. *Theo. Chem. Acc.* **2011**, *128*, 295-305.

53) Atkinson, R. Kinetics of the gas-phase reactions of OH radicals with alkanes and cycloalkanes. *Atmos. Chem. Phys.* **2003**, *3*, 2233-2307.

54) Rayez, M.T.; Rayez, J.C.; Sawerysyn, J.P. Ab initio studies of the reactions of chlorine atoms with fluoro- and chloro- substituted methanes. *J. Phys. Chem.* **1994**, *98*, 11342-11352.

55) Mendes, J.; Zhou, C.W.; Curran, H.J. Theoretical and kinetic study of the hydrogen atom abstraction reactions of esters with HO_2 radicals. *J. Phys. Chem. A* **2013**, *117*, 14006-14018.

56) Cometto, P.M.; Daële, V.; Idir, M.; Lane, S.I.; Mellouki, A. Reaction rate coefficients of OH radicals and Cl atoms with ethyl propanoate, n-propyl propanoate, methyl 2-methylpropanoate, and ethyl n-butanoate. *J. Phys. Chem. A* **2009**, *113*, 10745-10752.

57) Ifang, S.; Benter, T.; Barnes, I. Reactions of Cl atoms with alkyl esters: kinetic, mechanism and atmospheric implications. *Environ. Sci. Pollut. Res*. **2015**, *22*, 4820-4832.

58) Kwok, E.S.; Atkinson, R. Estimation of hydroxyl radical reaction rate constants for gas-phase organic compounds using a structure-reactivity relationship: an update. *Atmos. Environ.* **1995**, *29*, 1685-1695.

59) Cavalli, F.; Barnes, I.; Becker, K.H.; Wallington, T.J. Atmospheric oxidation mechanism of methyl propionate. *J. Phys*. *Chem*. *A*. **2000**, *104*, 11310-11317.

60) Christensen, L.K.; Ball, J.C.; Wallington, T.J. Atmospheric oxidation mechanism of methyl acetate. *J. Phys*. *Chem*. *A*. **2000**, *104*, 345-351.

61) Tuazon, E.C.; Aschmann, S.M.; Atkinson, R.; Carter, W.P. The reactions of selected acetates with the OH radical in the presence of NO: Novel rearrangement of alkoxy radicals of structure RC(O)OCH(Ȯ)Ŕ. *J. Phys*. *Chem*. *A*. **1998**, *102*, 2316-2321.

62) Andersen, V.F.; Ørnsø, K.B.; Jørgensen, S.; Nielsen, O.J.; Johnson, M.S. Atmospheric chemistry of ethyl propionate. *J. Phys*. *Chem*. *A*. **2012**, *116*, 5164-5179.

63) Wallington, T.J.; Ninomiya, Y.; Mashino, M.; Kawasaki, M.; Orkin, V.L.; Huie, R.E.; Kurylo, M.J.; Carter, W.P.L.; Luo, D.; Malkina, I.L. Atmospheric oxidation mechanism of methyl pivalate, $(CH_3)_3CC(O)OCH_3$. *J. Phys*. *Chem*. *A*. **2001**, *105*, 7225-7235.

64) Prinn, R.; Weiss, R.; Millar, B.; Jaung, J.; Alyea, F.; Cunnold, D.; Fraser, P.; Hartley, D.; Simmonds, P. Atmospheric trends and lifetime of CH_3CCI_3 and global OH concentrations. *Science* **1995**, *269*, 187-192.

65) Pinnock, S.; Hurley, M.D.; Shine, K.P.; Wallington, T.J.; Smyth, T.J. Radiative forcing of climate by hydrochlorofluorocarbons and hydrofluorocarbons. *J. Geophys*. *Res*. **1995**, *100*, 23227–23238.

66) Hodnebrog, O.; Etminan, M.; Fuglestvedt, J.S.; Marston, G.; Myhre, G.; Nielsen, C.J.; Shine, K.P.; Wallington, T.J. Global warming potentials and radiative efficiencies of halocarbons and related compounds: A comprehensive review. *Rev. Geophys.* **2013**, *51*, 300-378.

67) Schimel, D.; Alves, D.; Enting, I.; Heimann, M.; Joos, F.; Raynaud, D.; Wigley, T.; Prather, M.; Derwent, R.; Ehhalt, D.; Fraser, P. Radiative forcing of climate change. Climate change 1995: *The science of climate change* **1996**, 65-131.

68) Alecu, I.M.; Zheng, J.; Zhao, Y.; Truhlar, D.G. Computational thermochemistry: Scale factor databases and scale factors for vibrational frequencies obtained from electronic model chemistries. *J. Chem. Theory Comput.* **2010**, *6*, 2872-2887.

69) Bravo, I.; Aranda, A.; Hurley, M.D.; Marston, G.; Nutt, D.R.; Shine, K.P.; Smith, K.; Wallington, T.J. Infrared absorption spectra, radiative efficiencies, and global warming potentials of perfluorocarbons: Comparison between experiment and theory. *J. Geophys. Res.* **2010**, *115*, D24317.

70) Bravo, I.; Marston, G.; Nutt, D.R.; Shine, K.P. Radiative efficiencies and global warming potentials using theoretically determined absorption cross-sections for several hydrofluoroethers (HFEs) and hydrofluoropolyethers (HFPEs). *J. Quant. Spectrosc. Radiat. Transfer* **2011**, *112*, 1967-1977.

71) Jenkin, M.E. Photochemical ozone and PAN creation potentials: rationalization and methods of estimation. AEA technology plc. report AEAT-4182/20150/003. AEA Technology plc. National Environmental Technology Centre, Culham, Oxford shire OX14 3DB, U.K. **1998**.

72) Derwent, R.G.; Jenkin, M.E.; Saunders, S.M.; Pilling, M.J. Photochemical ozone creation potentials for organic compounds in North West Europe calculated with a master chemical mechanism. *Atmos. Environ.* **1998**, *32*, 2429–2441.
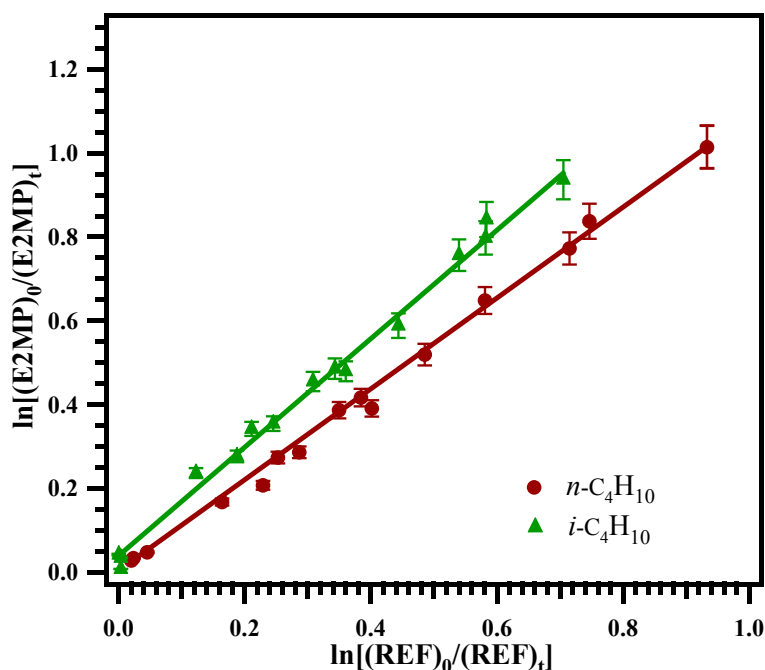
Figure 1a. Relative plot of the kinetic data for the OH radical initiated reaction with E2MP and relative to reference compounds at (298 ± 2) K at atmospheric pressure.
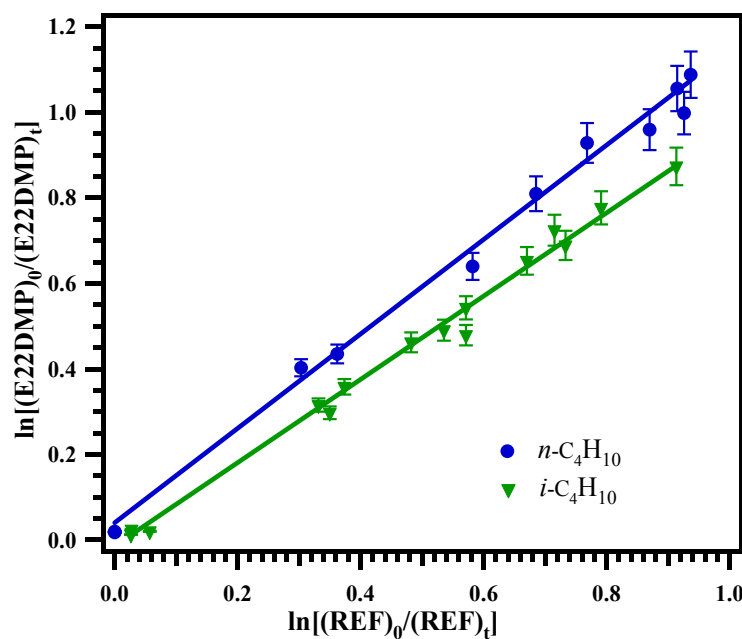

Figure 1b. Relative plot of the kinetic data for the OH radical initiated reaction with E22DMP and relative to reference compounds at (298 ± 2) K at atmospheric pressure.

Table 1a. Rate coefficients for the reaction of E2MP with OH radicals measured over the temperature range of 268-363 K and at atmospheric pressure. All the value of k is in the units of cm^3 molecule^{-1} s^{-1}.

T (K)	Reference	Bath gas	Slope±2σ	(Slope)$_{avg}$±2σ	(k_{E2MP}±2σ) ×10^{-12}	(k_{avg_E2MP}±2σ) ×10^{-12}
268±2	n-C$_4$H$_{10}$	N$_2$	1.84±0.01 1.86±0.03 1.80±0.01	1.84±0.03	3.74±0.87	3.44±1.10
	i-C$_4$H$_{10}$	N$_2$	1.61±0.10 1.68±0.01 1.66±0.03	1.65±0.11	3.14±0.73	
283±2	n-C$_4$H$_{10}$	N$_2$	1.57±0.02 1.61±0.01 1.57±0.05	1.59±0.06	3.39±0.76	3.17±0.99
	i-C$_4$H$_{10}$	N$_2$	1.49±0.01 1.49±0.05 1.49±0.04	1.49±0.06	2.95±0.65	
298±2	n-C$_4$H$_{10}$	N$_2$	1.03±0.01 1.08±0.05 1.10±0.04	1.07±0.06	2.52±0.53	2.71±0.79
	i-C$_4$H$_{10}$	N$_2$	1.34±0.02 1.36±0.04 1.39±0.01	1.37±0.05	2.90±0.59	
	n-C$_4$H$_{10}$	Air	1.13±0.05 1.18±0.10 1.20±0.15	1.17±0.18	2.75±0.70	2.78±0.96
	i-C$_4$H$_{10}$	Air	1.34±0.10 1.32±0.09 1.30±0.08	1.32±0.16	2.80±0.65	
313±2	n-C$_4$H$_{10}$	N$_2$	0.98±0.06 0.97±0.01 0.90±0.02	0.95±0.06	2.41±0.47	2.36±0.66
	i-C$_4$H$_{10}$	N$_2$	0.99±0.02 1.11±0.05 0.97±0.04	1.02±0.07	2.31±0.46	
	n-C$_4$H$_{10}$	N$_2$	0.77±0.03 0.79±0.07 0.77±0.01	0.78±0.08	2.30±0.43	

T (K)	Reference	Bath gas	Slope±2σ	(Slope)$_{avg}$±2σ	(k±2σ) ×10^{-12}	(k$_{avg}$±2σ) ×10^{-12}
343±2						2.23±0.57
	i-C$_4$H$_{10}$	N$_2$	0.86±0.01 0.85±0.01 0.83±0.05	0.85±0.05	2.16±0.38	
363±2	n-C$_4$H$_{10}$	N$_2$	0.69±0.01 0.65±0.06 0.71±0.03	0.68±0.07	2.21±0.39	
	i-C$_4$H$_{10}$	N$_2$	0.69±0.03 0.65±0.06 0.71±0.01	0.68±0.07	1.87±0.34	2.04±0.52

Table 1b. Rate coefficients for the reaction of E22DMP with OH radicals measured over the temperature range of 268-363 K and at atmospheric pressure. All the value of k is in the units of cm^3 molecule^{-1} s^{-1}.

T (K)	Reference	Bath gas	Slope±2σ	(Slope)$_{avg}$±2σ	(k$_{E22DMP}$± 2σ) ×10^{-12}	(k$_{avg\_E22DMP}$ ±2σ) ×10^{-12}
268±2	n-C$_4$H$_{10}$	N$_2$	1.68±0.02 1.63±0.04 1.67±0.05	1.66±0.07	3.38±0.80	3.31±1.09
	i-C$_4$H$_{10}$	N$_2$	1.71±0.05 1.72±0.05 1.70±0.01	1.71±0.07	3.24±0.74	
283±2	n-C$_4$H$_{10}$	N$_2$	1.35±0.11 1.32±0.09 1.34±0.02	1.34±0.14	2.86±0.70	2.86±0.96
	i-C$_4$H$_{10}$	N$_2$	1.44±0.10 1.46±0.06 1.49±0.03	1.45±0.12	2.86±0.66	
298±2	n-C$_4$H$_{10}$	N$_2$	1.10±0.02 1.13±0.05 1.20±0.06	1.14±0.08	2.68±0.57	2.58±0.80
	i-C$_4$H$_{10}$	N$_2$	1.20±0.08 1.17±0.02 1.14±0.09	1.17±0.12	2.48±0.56	
	n-C$_4$H$_{10}$	Air	1.12±0.13 1.14±0.05 1.13±0.02	1.13±0.14	2.66±0.63	

	$i\text{-}C_4H_{10}$	Air	1.21±0.15 1.22±0.07 1.19±0.10	1.21±0.19	2.56±0.66	2.61±0.91
313±2	$n\text{-}C_4H_{10}$	N_2	1.04±0.16 1.00±0.04 1.07±0.01	1.03±0.16	2.62±0.64	2.53±0.86
	$i\text{-}C_4H_{10}$	N_2	1.07±0.15 1.10±0.01 1.09±0.05	1.09±0.16	2.45±0.58	
343±2	$n\text{-}C_4H_{10}$	N_2	0.81±0.13 0.89±0.08 0.83±0.12	0.84±0.20	2.49±0.71	2.24±0.86
	$i\text{-}C_4H_{10}$	N_2	0.75±0.02 0.80±0.11 0.80±0.12	0.79±0.16	2.00±0.53	
363±2	$n\text{-}C_4H_{10}$	N_2	0.60±0.02 0.60±0.08 0.60 ±0.13	0.60±0.15	1.94±0.57	1.81±0.65
	$i\text{-}C_4H_{10}$	N_2	0.61±0.02 0.60±0.07 0.61±0.04	0.61±0.08	1.67±0.34	
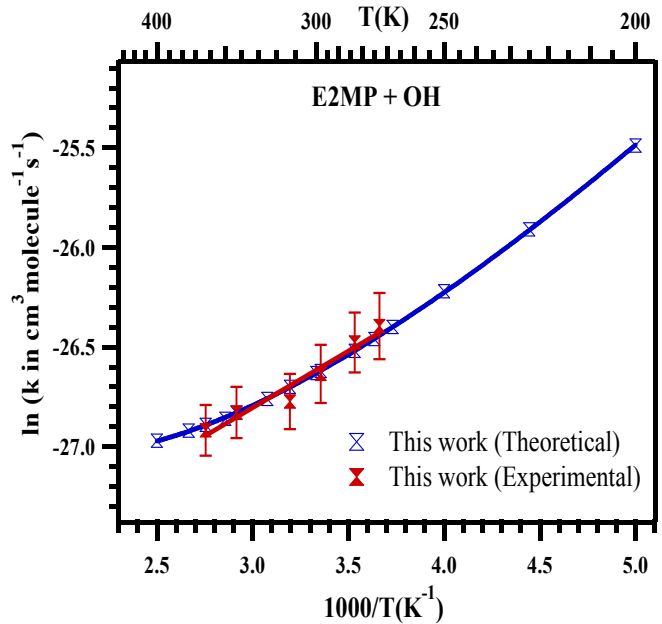
Figure 2a. Arrhenius plots for the rate coefficients measured for the reaction of E2MP with OH radicals along with calculated rate coefficients in the temperature range of 200-400 K.
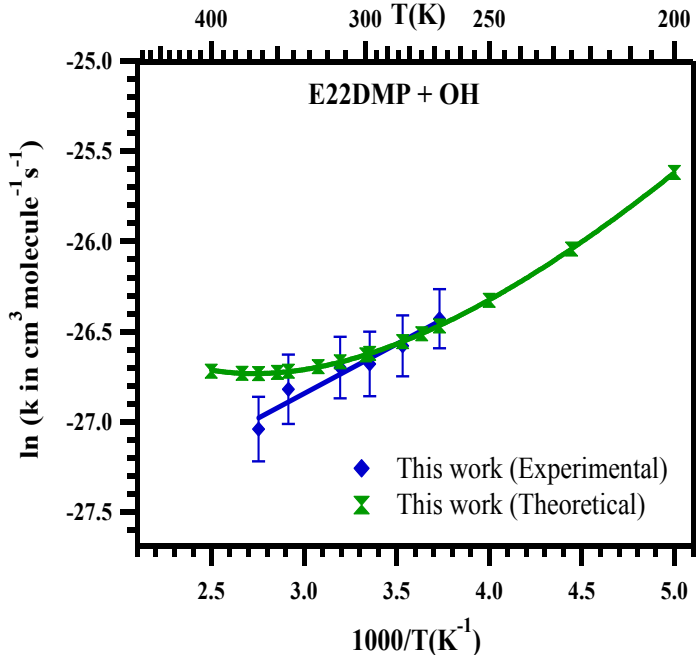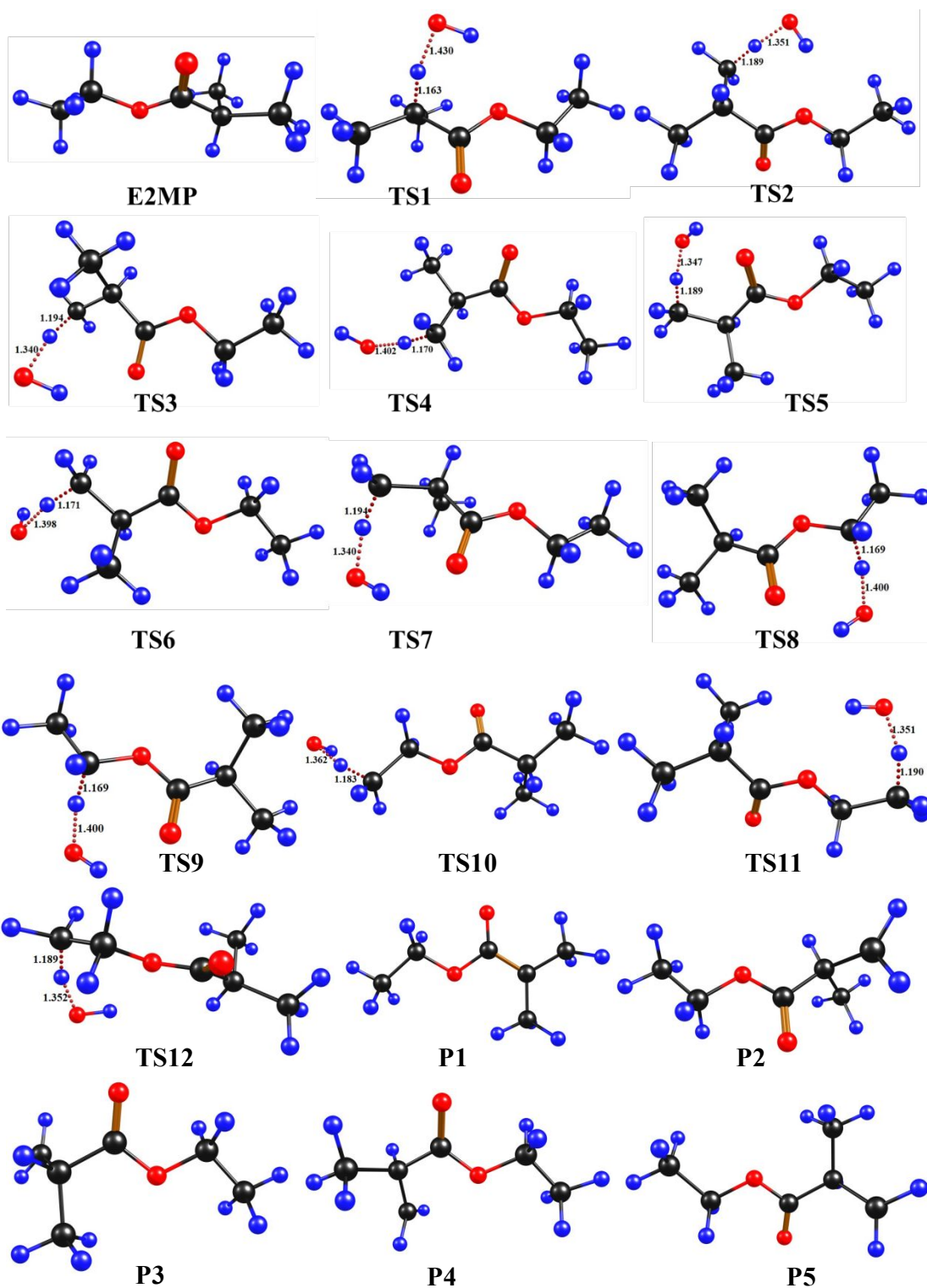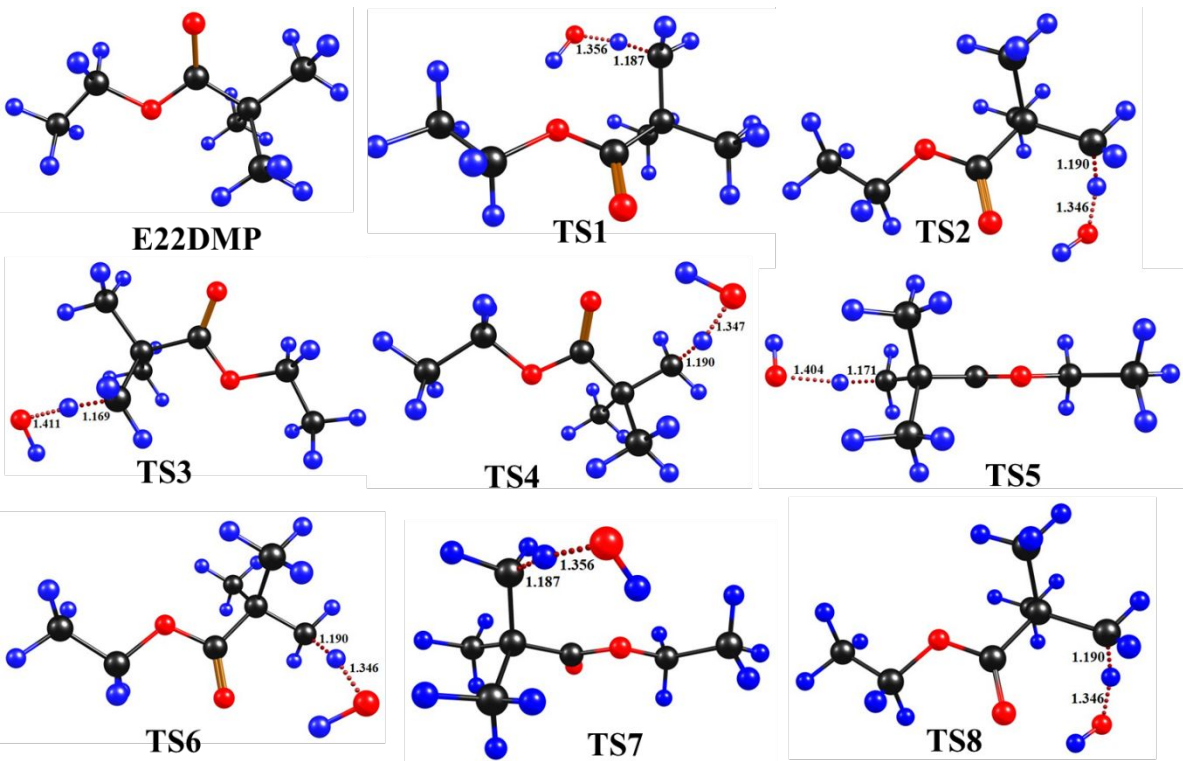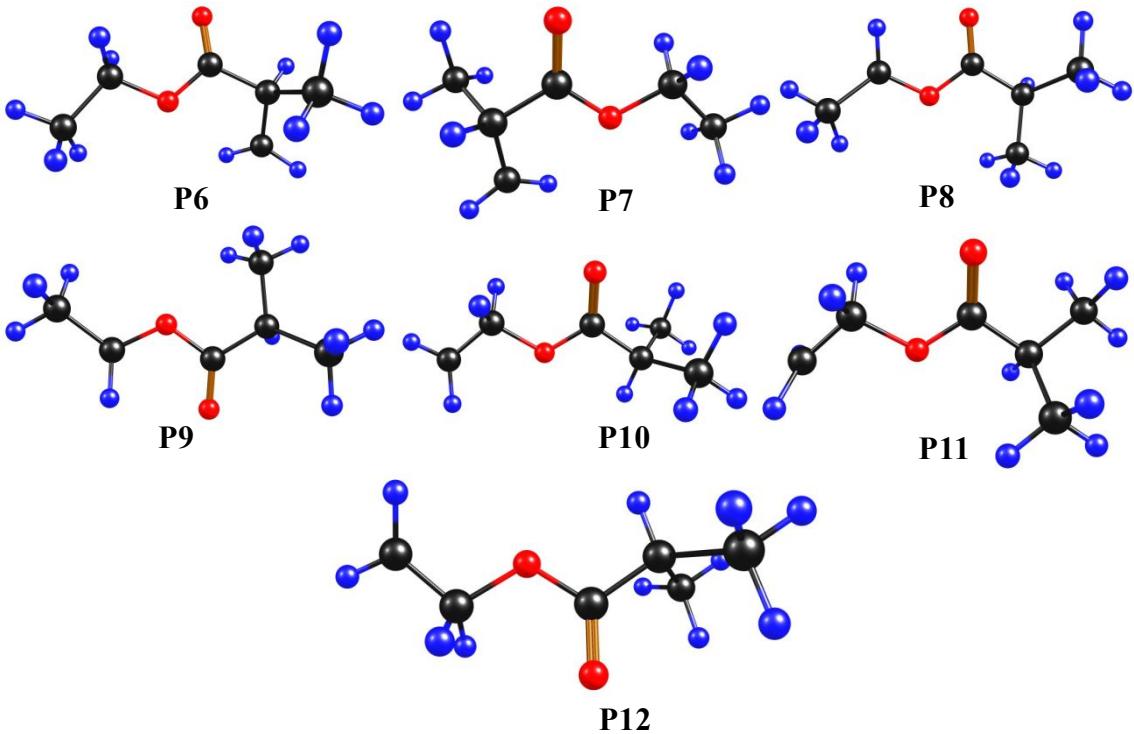

Figure 2b. Arrhenius plots for the rate coefficients measured for the reaction of E2MP with OH radicals along with calculated rate coefficients in the temperature range of 200-400 K.

E2MP

TS1

TS2

TS3

TS4

TS5

TS6

TS7

TS8

TS9

TS10

TS11

TS12

P1

P2

P3

P4

P5

P6

P7

P8

P9

P10

P11

P12

E22DMP

TS1

TS2

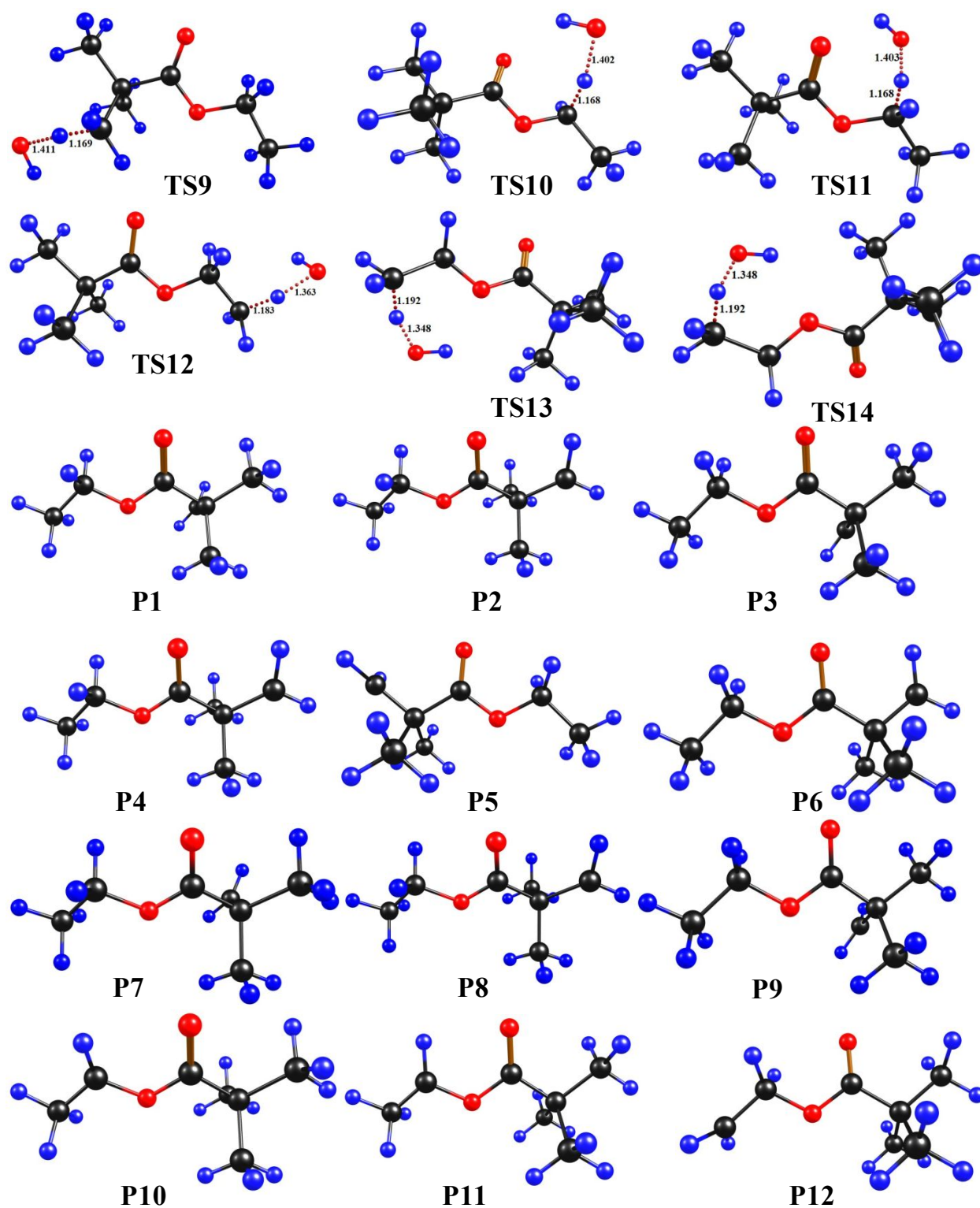**TS3**

TS4

TS5

TS6

TS7

TS8

Figure 3. Optimized geometries of reactants (E2MP and E22DMP), transition states (TS), products (P) for the title reactions obtained at M06-2X/6-311++G(d,p) level of theory.
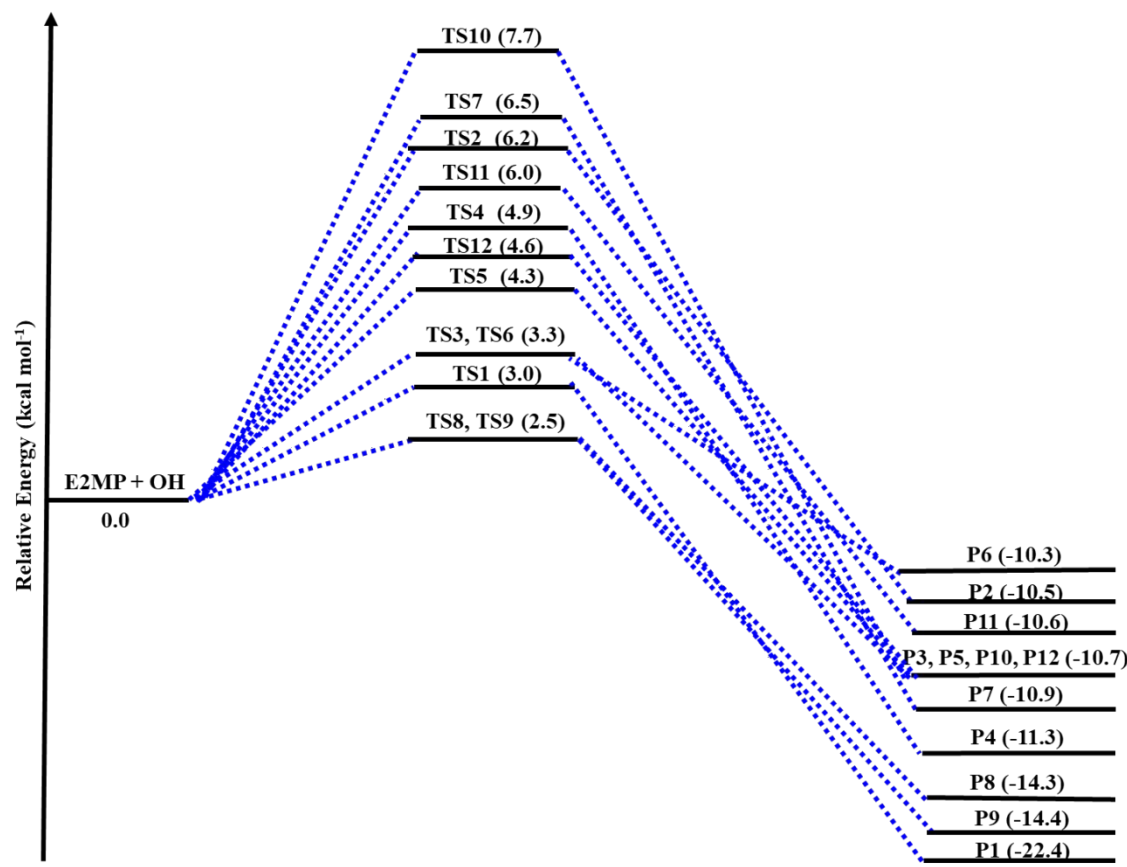
Figure 4a. PES for the reaction of E2MP with OH radicals obtained at CCSD(T)/cc-pVTZ//M06-2X/6-311++G(2d,2p) level of theory.
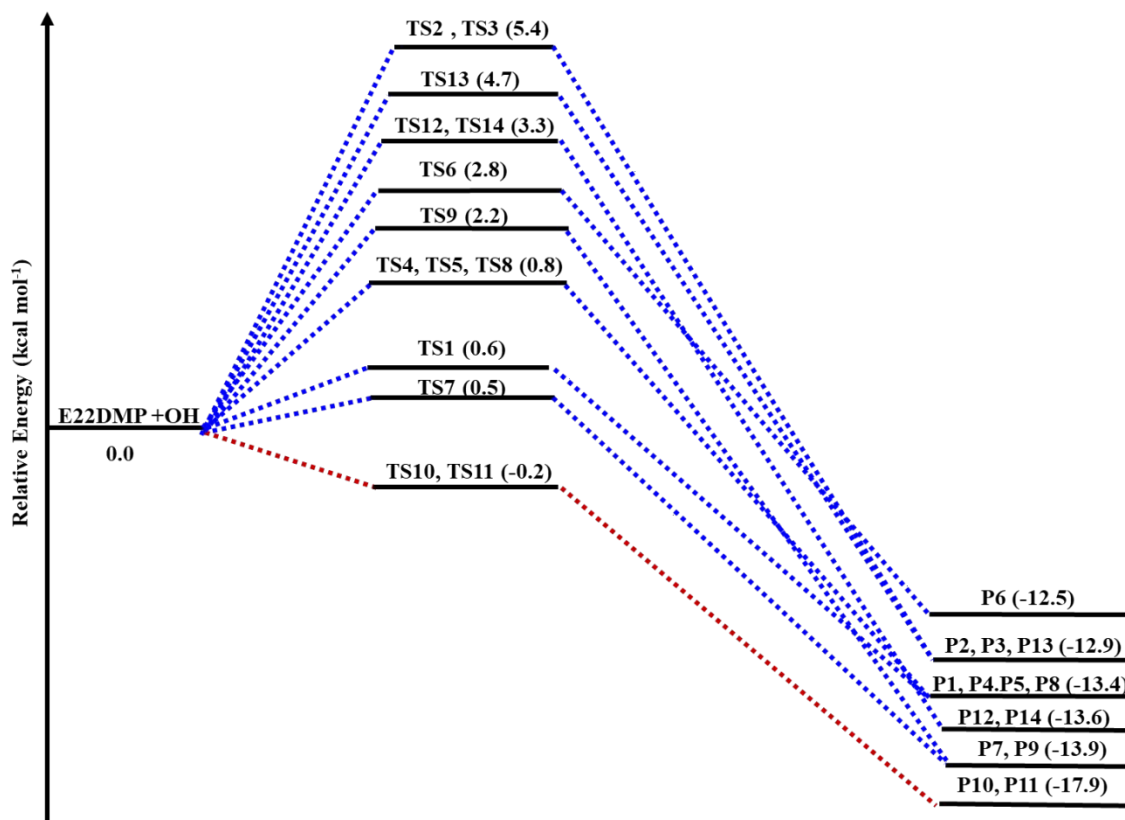
Figure 4b. PES for the reaction of E22DMP with OH radicals obtained at CCSD(T)/cc-pVTZ//M06-2X/6-311++G(2d,2p) level of theory.

Table 2a. Thermochemical parameters [standard changes in enthalpies (ΔH°) and standard change in free energies (ΔG°) are in the unit of kcal mol^{-1}] and L-parameter for the reaction of E2MP with OH radical were obtained at M06-2X/6-311++G(2d,2p) level of theory.

TS	ΔG°	ΔH°	L-parameter
TS1 (C1)	-29.8	-28.5	0.14
TS2 (C2a)	-15.6	-15.3	0.23
TS3 (C2b)	-14.9	-15.4	0.18
TS4 (C2c)	-15.4	-15.7	0.23
TS5 (C3a)	-14.9	-15.4	0.23
TS6 (C3b)	-14.9	-15.1	0.18
TS7 (C3c)	-17.3	-14.8	0.26
TS8 (C4a)	-19.3	-19.9	0.16
TS9 (C4b)	-19.3	-19.9	0.16
TS10 (C10a)	-14.7	-15.3	0.22

TS11 (C11b)	-14.7	-15.3	0.25
TS12 (C12c)	-16.2	-15.2	0.28

Table 2b. Thermochemical parameters [standard changes in enthalpies (ΔH°) and standard change in free energies (ΔG°) are in the unit of kcal mol^{-1}] and L-parameter for the reaction of E22DMP with OH radical were obtained at M06-2X/6-311++G(2d,2p) level of theory.

TSs	ΔG°	ΔH°	L-parameter
TS1 (C6a)	-16.4	-15.0	0.23
TS2 (C6b)	-16.5	-14.3	0.22
TS3 (C6c)	-16.5	-14.3	0.22
TS4 (C7a)	-16.4	-15.0	0.26
TS5 (C7b)	-16.4	-15.0	0.26
TS6 (C7c)	-15.7	-14.2	0.18
TS7 (C8a)	-16.7	-15.6	0.23
TS8 (C8b)	-16.4	-15.0	0.26
TS9 (C8c)	-16.7	-15.6	0.23
TS10 (C9a)	-21.2	-20.1	0.18
TS11 (C9b)	-21.2	-20.1	0.18
TS12 (C10a)	-16.2	-15.0	0.22
TS13 (C10b)	-16.4	-14.3	0.25
TS14 (C10c)	-16.2	-15.0	0.22

Table 3. Comparison of the measured rate coefficients with calculated kinetic for the reactions of

E2MP and E22DMP with OH radicals.

| T(K)	$k \times 10^{12}$ (in cm^3 molecule^{-1} s^{-1})		Relative rate coefficient (k in cm^3 molecule^{-1} s^{-1})	
	E2MP	E22DMP	E2MP $\times 10^{-12}$	E22DMP $\times 10^{-12}$
200	9.07×10^{-12}	7.48×10^{-12}		
225	5.99×10^{-12}	4.89×10^{-12}		
250	4.41×10^{-12}	3.68×10^{-12}		
268	3.72×10^{-12}	3.19×10^{-12}	3.44±1.10	3.31±1.09
275	3.52×10^{-12}	3.06×10^{-12}		
283	3.31×10^{-12}	2.93×10^{-12}	3.17±0.99	2.86±0.96
298	3.01×10^{-12}	2.82×10^{-12}	2.71±0.79	2.58±0.80
300	2.98×10^{-12}	2.72×10^{-12}		
313	2.78×10^{-12}	2.62×10^{-12}	2.36±0.66	2.53±0.86
325	2.63×10^{-12}	2.55×10^{-12}		
343	2.46×10^{-12}	2.49×10^{-12}	2.23±0.57	2.24±0.86
350	2.41×10^{-12}	2.47×10^{-12}		
363	2.36×10^{-12}	2.46×10^{-12}	2.04±0.52	1.81±0.65
375	2.26×10^{-12}	2.46×10^{-12}		
400	2.17×10^{-12}	2.49×10^{-12}		
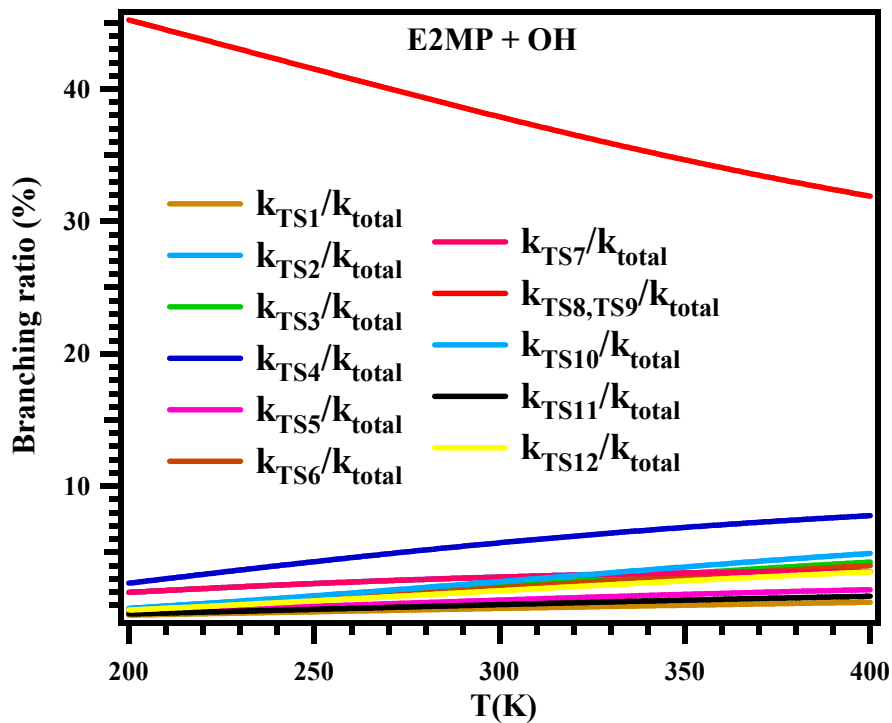
Figure 5a. Plots for the contribution of each reaction channel to the total reactivity for the reaction
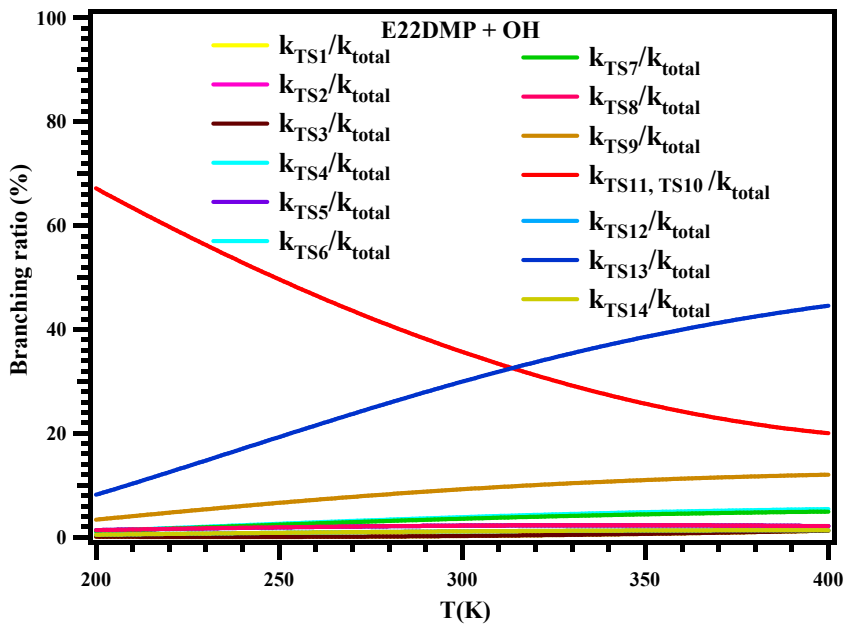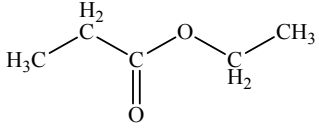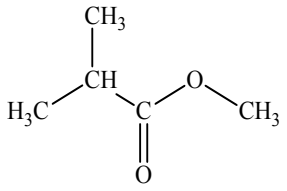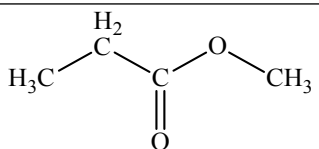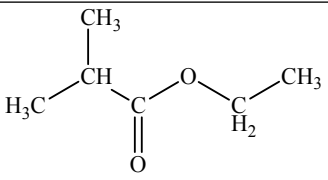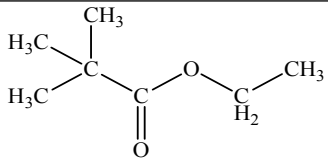
of E2MP with OH radicals.

Figure 5b. Plots for the contribution of each reaction channel to the total reactivity for the reaction

of E22DMP with OH radicals.

Table 4. Comparison of the kinetics (k, in units of cm^3 molecule^{-1} s^{-1}) measured for the reactions of E2MP and E22DMP with OH radicals at 298 K with the available literature data.

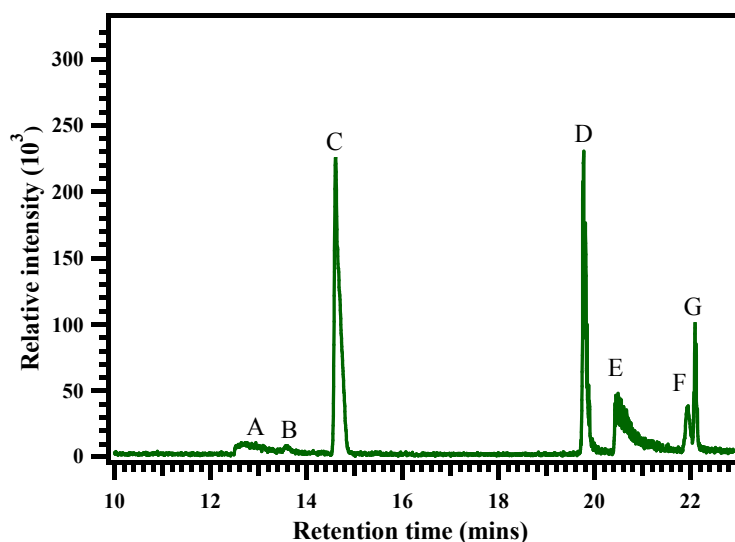| Ester	$k \times 10^{12}$	Experimental Technique	Reference
 Ethyl propionate(EP)	2.40± 0.10	PLP-LIF	Cometto et al.[56]
 Methyl-2-methyl propionate (M2MP)	5.10 ± 0.50		
 Methyl propionate (MP)	0.83 ± 0.09	PLP-LIF	Le Calve et al.[14]
 Ethyl-2-methyl propionate (E2MP)	2.71 ± 0.79	RR	This work
	3.80	SAR	
 Ethyl-2,2-dimethyl propionate (E22DMP)	2.58 ± 0.80	RR	
	1.72	SAR	

Figure 6a. GC-MS chromatogram for the reaction of E2MP with OH radicals. The alphabets given in the chromatogram are the products identified in the GC-MS. The products are A) CO_2 B) Formaldehyde C) Acetaldehyde D) Acetone E) Methanol F) propene and G) Ethyl formate.
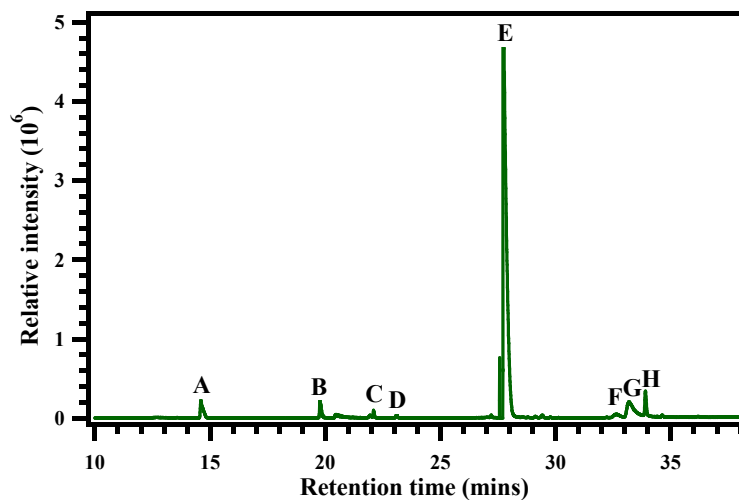

Figure 6b. GC-MS chromatogram for the reaction of E22DMP with OH radicals. The alphabets given in the chromatogram are the products identified in the GC-MS. The products are A) CO_2 B) HCHO C) Methanol D) 2-methyl-propene E) Acetaldehyde F) Acetone G) Ethyl formate and H) Acetic acid formic anhydride.
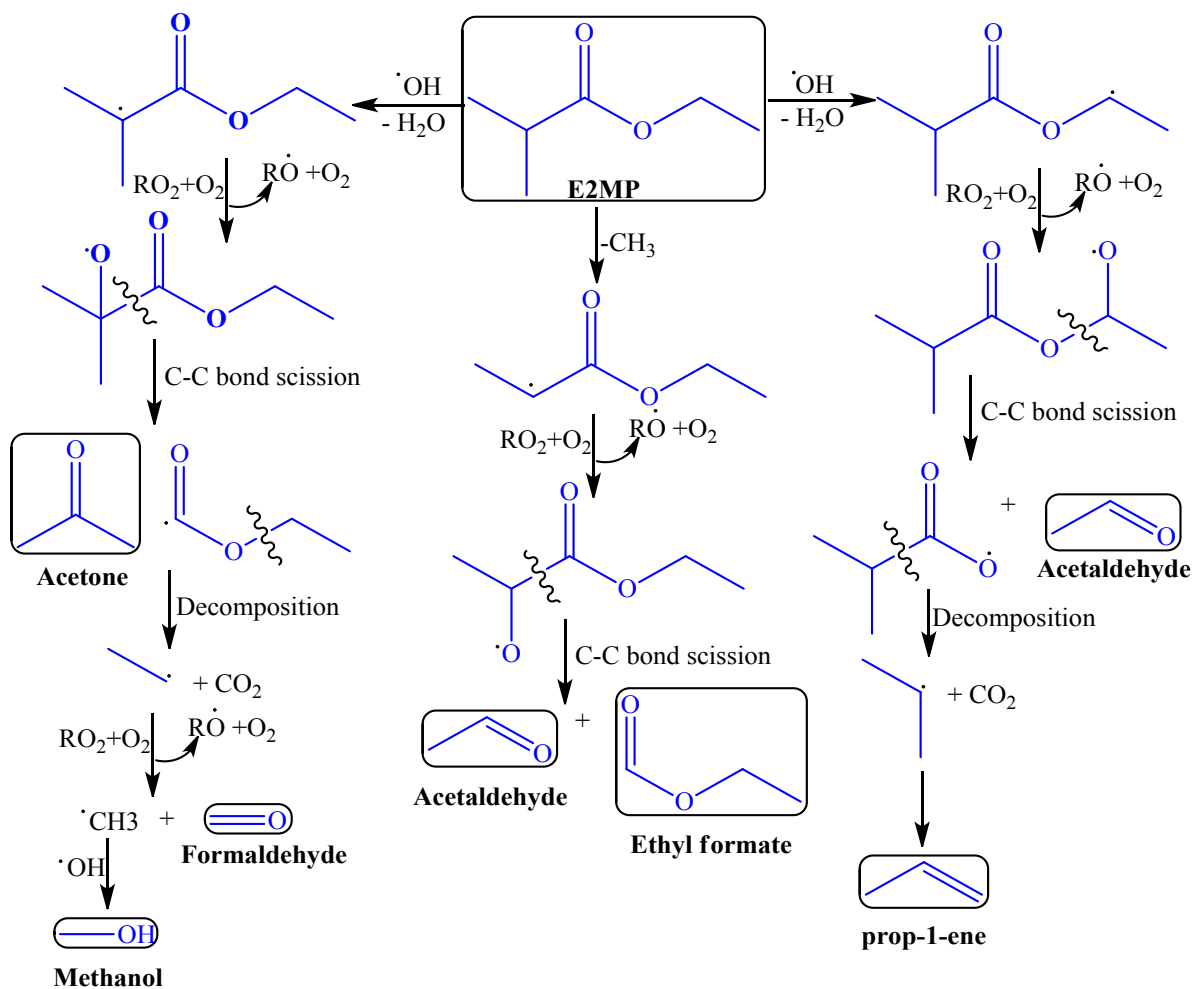
Figure 7a. Predicted product degradation mechanism for the reaction of E2MP with OH radicals.

1
2
3
4
5
6
7
8
9
10
11
12
13
14
15
16
17
18
19
20
21
22
23
24
25
26
27
28
29
30
31
32
33
34
35
36
37
38
39
40
41
42
43
44
45
46
47
48
49
50
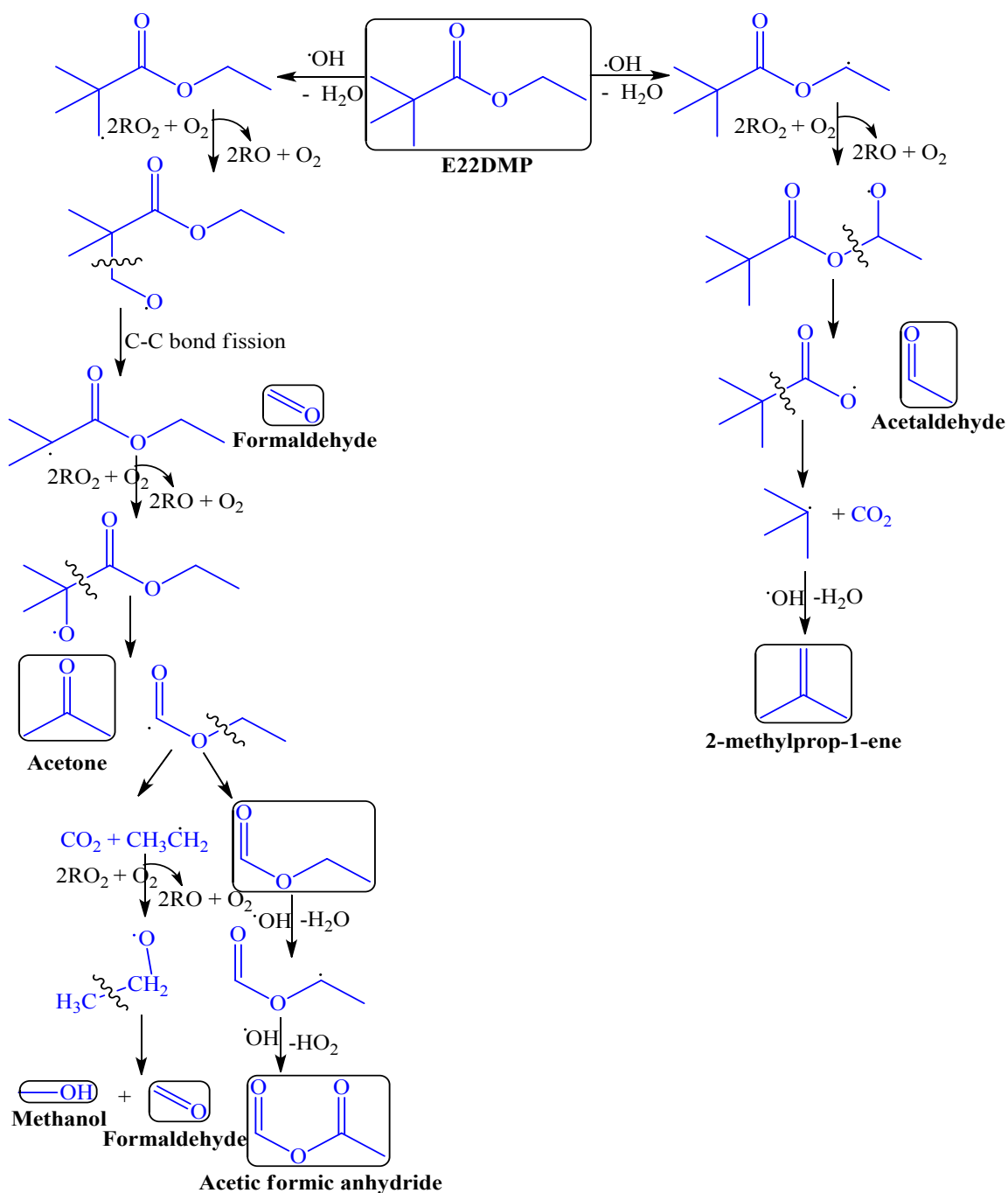51
52
53
54
55
56
57
58
59
60

Figure 7b. Predicted product degradation mechanism for the reaction of E22DMP with OH radicals.

Table 5. Atmospheric lifetimes in days, RFs, lifetime corrected RFs, GWPs and POCPs for the reaction of E2MP and E22DMP with OH radicals.

Ester	Atmospheric Lifetimes (in hours)	RFs	Lifetime corrected RFs	GWPs		
	$[OH] = 1 \times 10^6$ molecules cm^{-3}			20 years	100 years	500 years
E2MP	92	0.14	0.04	0.8	0.2	0.1
E22DMP	105	0.72	0.20	3.9	1.0	0.5
POCPs						
	n_B	n_c	M	γ_s	γ_R	POCP
E2MP	17	6	116.16	0.681	0.117	33.9
E22DMP	19	7	130.18	0.680	0.094	30.9

TOC Graphics

Ethyl-2-methyl propionate

Ethyl-2,2-dimethyl propionate

+ OH

T=268-363 K, Experiment

T=200-400 K, Theory

Products